MOBILITY MANAGEMENT AND RESOURCE ALLOCATION STRATEGIES FOR VISIBLE LIGHT COMMUNICATION NETWORKS

A Dissertation

by

M. Selim Demir

Submitted to the
Graduate School of Sciences and Engineering
In Partial Fulfillment of the Requirements for
the Degree of

Doctor of Philosophy

in the
Department of Electrical and Electronics Engineering

Özyeğin University
May 2021

MOBILITY MANAGEMENT AND RESOURCE ALLOCATION STRATEGIES FOR VISIBLE LIGHT COMMUNICATION NETWORKS

Approved by:

Prof. Murat Uysal, Advisor
Department of Electrical and Electronics Engineering
Özyeğin University

Prof. Sinem Çöleri
Department of Electrical and Electronics Engineering
Koç University

Prof. H. Fatih Uğurdağ
Department of Electrical and Electronics Engineering
Özyeğin University

Prof. İbrahim Altunbaş
Department of Electronics and Communication Engineering
İstanbul Technical University

Date Approved: 11 May 2021

Assoc. Prof. Hacı İlhan
Department of Electronics and Communication Engineering
Yıldız Technical University

To my family

ABSTRACT

There has been a growing interest in Visible Light Communications (VLC) in recent years. The existing works in the literature on point-to-point VLC systems are well established, and especially the studies on physical layer aspects demonstrate the potential of VLC. However, to transform VLC into a multi-user, multi-cell, scalable, and fully networked wireless technology, significant further efforts for upper layer issues are needed. This dissertation focuses on mobility management and resource allocation techniques for indoor and vehicular VLC systems. In the first part of this thesis, we consider a centralized Direct Current biased Optical Orthogonal Frequency Division Multiplexing (DCO-OFDM) based VLC network and formulate a subcarrier resource allocation problem to maximize the user satisfaction index. We have used the Particle Swarm Optimization (PSO) method for the solution to the resulting problem. The superiority of the proposed algorithm is demonstrated through an extensive simulation study. In the second part of the thesis, we propose an energy-efficient dynamic resource management framework for indoor OFDM-based VLC networks. Specifically, we formulate and investigate a stochastic cross-layer optimization problem to optimize the network resources under the constraints of queue stability and power to maximize the average system throughput. In the last part of the thesis, we propose handover algorithms for indoor and outdoor VLC networks. First, we propose a handover algorithm for indoor VLC networks with Coordinated Multipoint (CoMP) transmission and evaluate its performance in physical channel settings based on ray tracing. Then, we present a novel dynamic handover algorithm for outdoor vehicular VLC networks. The proposed algorithm dynamically revises the handover parameters by considering the vehicle speed without requiring additional feedback information.

ÖZETÇE

Görünür ışık haberleşmesi (VLC) sistemlerine son yıllarda giderek artan bir ilgi mevcuttur. Literatürdeki noktadan noktaya VLC sistemlerini inceleyen çalışmalar yeterli olgunluk seviyesindedir ve özellikle fiziksel katman ile ilgili çalışmalar VLC'nin potansiyelini ortaya koymaktadır. Fakat, VLC sistemlerini çok kullanıcılı, çok hücreli ve ağ tabanlı bir kablosuz ağ teknolojisine dönüştürmek için üst katman konularını inceleyen önemli yeni çalışmalara ihtiyaç vardır. Bu tez iç mekan ve taşıtlara ilişkin VLC sistemlerinde kaynak ataması ve hareketlilik yönetimi tekniklerine odaklanır. Bu tezin ilk kısmında, doğru akım eşikli optik ortogonal frekans bölmeli çoğullama (DCO-OFDM) tekniğine dayalı merkezi bir VLC ağı için kullanıcı memnuniyet indeksini maksimize eden bir alt taşıyıcı atama problemi formüle edilmiştir. Bu problemin çözümü için biyolojiden ilham alan parçacık sürü optimizasyonu (PSO) kullanılmıştır. Önerilen algoritmanın üstünlüğü kapsamlı bir simülasyon çalışmasıyla gösterilmiştir. Tezin ikinci kısmında, OFDM temelli iç mekan VLC ağları için enerji tasarruflu dinamik kaynak yönetimi yapısı önerilmiştir. Spesifik olarak, kuyruk kararlılığı ve güç kısıtları altında ortalama sistem çıktısını maksimize etmek için ağ kaynaklarının kullanımını en iyileyen stokastik katmanlar arası optimizasyon problemi formüle edilmiş ve incelenmiştir. Tezin son kısmında, iç ve dış mekan VLC ağları için el değiştirme yöntemleri önerilmiştir. İlk olarak, iç mekan VLC ağları için koordineli çok-noktalı (CoMP) iletimli bir el değiştirme algoritması önerilmiş ve önerilen algoritmanın performansı ışın takibine dayalı fiziksel kanal kullanılarak değerlendirilmiştir. Sonrasında, taşıtlara ilişkin VLC ağları için hıza duyarlı dinamik bir el değiştirme yöntemi gösterilmiştir. Önerilen algoritma, ek geri bildirim bilgisi gerektirmeden araç hızını dikkate alarak el değiştirme parametrelerini dinamik olarak revize eder.

ACKNOWLEDGEMENTS

I feel myself extremely lucky to have the privilege and great honor of working with my thesis advisor, Prof. Murat Uysal. I have learned so much from his broad technical knowledge and research philosophy and his incredible humility, generosity, and kindness. I would like to thank him for his guidance, generous support, and encouragement throughout my PhD research. I will never forget his support and for providing me numerous opportunities to learn and develop as a researcher.

I thank Prof. H. Fatih Uğurdağ for his invaluable support and helpful feedback throughout my PhD research and for his time serving on my thesis committee and carefully reviewing my dissertation. I would also like to express my gratitude to the other members of my thesis committee, Assoc. Prof. Hacı İlhan, Prof. Sinem Çöleri, and Prof. Dr. İbrahim Altunbaş, who found the time in their busy schedules to review my thesis and provide valuable feedback.

I would like to thank my colleagues at TÜBİTAK BİLGEM, namely, Dr. İbrahim Hökelek, Dr. Ömer Faruk Gemici, and Dr. Serdar Özgür Ata for the daily discussions and their invaluable feedback on my research.

My warmest gratitude goes to my mother and father for their love and encouragement. I cannot thank them enough for all they have given me. I would like to especially thank my brothers for their continuous support. This would have been all be much more difficult without their help.

Last but certainly not least, I would like to thank my precious children Elif Sevde and Ali Tahir, who make every day of my life beautiful. I must express my gratitude to my wonderful wife for her encouragement and sacrifice during the last few years.

TABLE OF CONTENTS

LIST OF TABLES

LIST OF FIGURES

GLOSSARY

AP	Access point
ACO-OFDM	Asymmetrically clipped optical OFDM
BC	Best Connection
CDF	Cumulative distribution function
CIR	Channel impulse response
CoMP	Coordinated multipoint
CoMP-JP	CoMP-Joint Processing
CQI	Channel quality information
CSI	Channel state information
CU	Control unit
C-LiAN	Centralized light access network
DCO-OFDM	Direct current biased optical OFDM
DCO-OFDMA	Direct current biased optical OFDMA
DD	Direct detection
FOV	Field-of-view
GA	Genetic algorithm
HOM	Handover margin
I2V	Infrastructure-to-vehicle
IDFT	Inverse discrete Fourier transform
IFFT	Inverse fast Fourier transform
IM	Intensity modulation
IM/DD	Intensity modulation direct detection
ISI	Inter-symbol interference
ITS	Intelligent transportation systems
JT-HO	Joint transmission handover

LED	Light emitting diode
LOS	Line-of-sight
MAC	Medium access control
MPPM	Multipulse pulse position modulation
OCDMA	Optical code division multiple access
OFDM	Orthogonal frequency division multiplexing
OFDMA	Orthogonal frequency division multiple access
OOK	On-off keying
OPPM	Overlapping pulse position modulation
PAM	Pulse amplitude modulation
PD	Photodetector
PHY	Physical layer
PPM	Pulse position modulation
PSD	Power spectral density
PSK	Phase-shift keying
PSO	Particle swarm optimization
PWM	Pulse width modulation
QAM	Quadrature amplitude modulation
QoS	Quality-of-service
QSI	Queue state information
RF	Radio frequency
RR	Round Robin
RWP	Random waypoint model
SDMA	Space division multiple access
SINR	Signal to interference plus noise ratio

SNR	Signal to noise ratio
TDMA	Time division multiple access
TTT	Time-to-trigger
V2I	Vehicle-to-infrastructure
V2V	Vehicle-to-vehicle
VLC	Visible light communication
VPPM	Variable pulse position modulation

CHAPTER I

INTRODUCTION

Visible Light Communication (VLC) has emerged as a complementary short-range wireless access technique based on the dual use of Light Emitting Diodes (LEDs). VLC uses the unregulated visible light spectrum from 380 nanometer to 780 nanometer with hundreds of terahertz bandwidth for signal transmission (see Fig. 1.1 [1]). In VLC systems, light from LEDs is modulated at high speeds not noticeable to the human eye without any adverse effects on illumination levels. Therefore, low cost and energy efficient LEDs can provide wireless access to multiple users as an add-on service to the primary task of illumination [2].

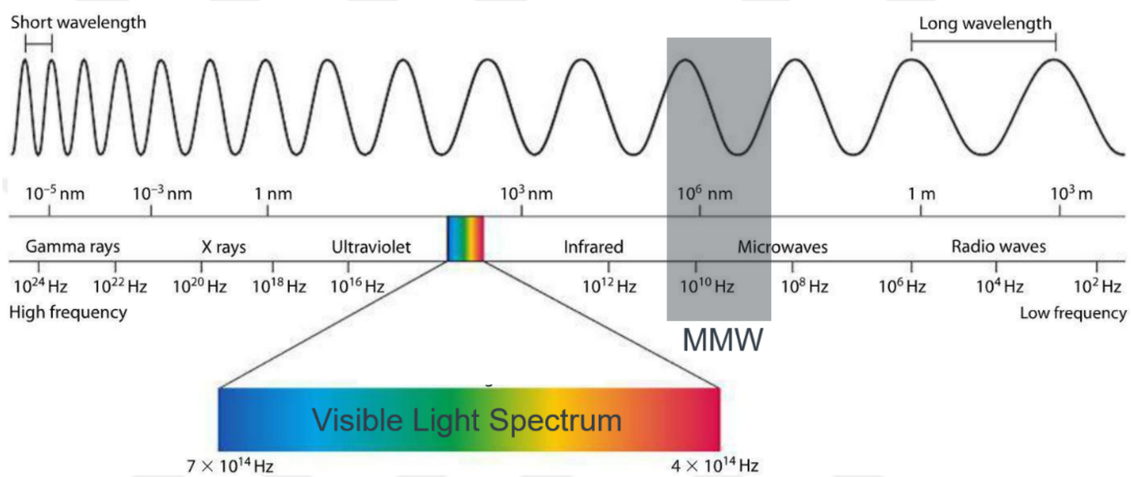

Figure 1.1: Electromagnetic spectrum.

Unlike other wireless communication technologies, VLC is non-hazardous to human health. Furthermore, VLC systems do not affect the functionality of the high sensitive electronic systems; therefore, they can be used in electromagnetic sensitive areas (e.g., airplanes, hospitals, chemical or nuclear plants). VLC is also an energy-efficient solution, where the light is used for both illumination and data transmission [3].

Typical VLC systems use LEDs as transmitters and the main element in the receiver is the Photo-Detector (PD). Photodiode and the phototransistors are two main types of PDs used in VLC receivers to collect the light radiation. In the receiver part of the VLC systems a PD demodulates the light signal into electrical signals. Thus, Intensity Modulation and Direct Detection (IM/DD) is employed for data transmission. Since the instantaneous radiated optical power is determined by the amplitude of the signal, the VLC signal needs to be real-valued and non-negative. These constraints limit the usage of conventional modulation schemes used in radio frequency based communication systems. Initial studies in VLC systems considered simple pulse modulation techniques such as Pulse Position Modulation (PPM) and On-Off Keying (OOK). Recent works have adopted Orthogonal Frequency Division Multiplexing (OFDM) for VLC systems. In order to obtain unipolar and real OFDM signals some favorable techniques for VLC systems are reported such as Direct Current biased Optical OFDM (DCO-OFDM) and Asymmetrically Clipped Optical OFDM (ACO-OFDM) [4].

Potential applications of VLC include indoor wireless communication, underwater communication, vehicle to vehicle communication, positioning systems and robotics [5]. VLC is envisioned to provide high data rate internet access for indoor environments but not intended to replace the existing WiFi or mobile networks. Rather, it is an alternative wireless data link, where radio transmission is not desired, not possible, or not sufficient [6].

VLC can be used for vehicular communication due to the existing presence of the vehicle lights and the traffic light infrastructure. In the context of vehicular networking, automotive headlight, street and traffic lamps can be potentially used as VLC transmitters. In particular, uniformly placed highway street lights provide the required infrastructure for the implementation of infrastructure-to-vehicle communication networks.

1.1 Channel Models

In this section, we first present the analytical VLC channel model. Then we highlight the shortcomings of the analytical channel model and present the ray tracing based physical channel modeling approach.

1.1.1 Analytical LOS Model

A commonly deployed VLC channel model in the literature is the analytical channel based on Line-of-Sight (LOS), see Fig. 1.2. The channel coefficient for this model is expressed as

$$H = \begin{cases} \dfrac{(m+1)\,AR}{2\pi d^2} \cos^m(\phi)\cos(\psi), & 0 \le \psi \le \Psi_{1/2} \\ 0, & \psi > \Psi_{1/2} \end{cases} \tag{1.1}$$

where A denotes the PD area, d denotes the distance between the corresponding LED and PD pair, R is the responsivity of the PD, ϕ is the angle of irradiance, ψ is the angle of incident and $\Psi_{1/2}$ is the Field-of-View (FOV) semi-angle of the PD. In (1.1), $m = -\ln 2/\ln(\cos(\Phi_{1/2}))$ is the order of Lambertian emission, where $\Phi_{1/2}$ denotes the semi-angle of the LED.

1.1.2 Ray Tracing Based Physical Model

The LOS channel model is limited to the assumption of a Lambertian source and does not take into account the effect of reflections. Ray-tracing based approaches allow to precisely take into account the characteristics of propagation environment (i.e., presence of human beings, objects, etc), light sources (i.e., beamshape) and detectors (i.e., rotation, field-of-view, etc). By using the non-sequential ray tracing features of Zemax® and calculating the detected power and path lengths from source to detector for each ray, the optical Channel Impulse Response (CIR) can be obtained [7].

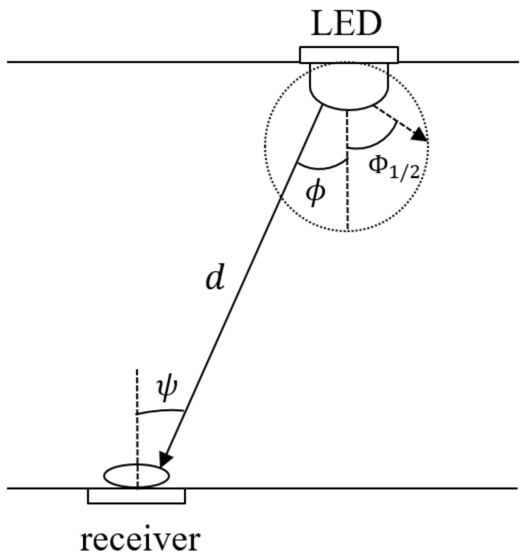

Figure 1.2: VLC downlink transmission geometry.

Let $h(t)$ denote the optical CIR between the corresponding LED and the receiver. It can be expressed as

$$h(t) = \sum_{j=1}^{N_r} P_j \ \delta(t - \tau_j), \tag{1.2}$$

where P_j is the optical power of the j^{th} ray from the corresponding LED, τ_j is the propagation time of the j^{th} ray from the corresponding LED, $\delta(t)$ is the Dirac delta function and N_r is the number of rays received at the detector. Under the assumption that sampling interval is much higher than delay spread, the multipath components are not resolvable and the channel can be modeled as a single coefficient given by

$$H = \int_0^\infty h(t)dt. \tag{1.3}$$

1.2 Modulation Techniques

LEDs are incoherent sources and cannot generate a beam of photons with the same frequency and constant phase difference. Since light signal generated by LEDs are incoherent and it is difficult to capture a stable carrier, IM/DD is used for data transmission in VLC [8]. In Intensity Modulation (IM), the instantaneous power of the carrier is in accordance with the waveform of modulating signal. In Direct Detection

(DD), a PD proportionally converts the received instantaneous optical power to a current. Unlike RF systems, the transmitted signals in VLC systems need to be real-valued and non-negative. Therefore, modulation techniques used in RF systems require modification before they can be applied to VLC systems. In order to do so, single-carrier and multi-carrier modulation techniques have been well studied and practiced for VLC systems [9].

1.2.1 Single carrier

Single carrier modulation techniques have some advantages over multi-carrier modulation techniques, such as having low complexity, achieving better performance in flat channels and being more resistant to nonlinear distortions at an optical transmitter. Single carrier modulation techniques are suitable for low-speed applications. However, at high data rates implementing these modulation schemes requires complex equalizers. Real-valued single carrier modulation techniques can be modified from RF to VLC with few changes. Details of these modulation techniques including unipolar OOK, PPM, Pulse Width Modulation (PWM), and Pulse Amplitude Modulation (PAM) are given as follows.

1.2.1.1 OOK

OOK is a very simple binary level modulation technique that is used in IM/DD VLC systems. In OOK signaling, modulated data is represented by the presence or absence of a light pulse in each symbol interval. When a pulse occurs in a symbol period, bit "1" is transmitted while bit "0" is transmitted if there is no pulse in the symbol period. OOK-like modulation is widely used in wireline communication systems. The major advantage of OOK is its ease of implementation, but its low data rates, especially while supporting different dimming levels, is an important limiting factor [10]. OOK has relatively poor energy and spectral efficiency.

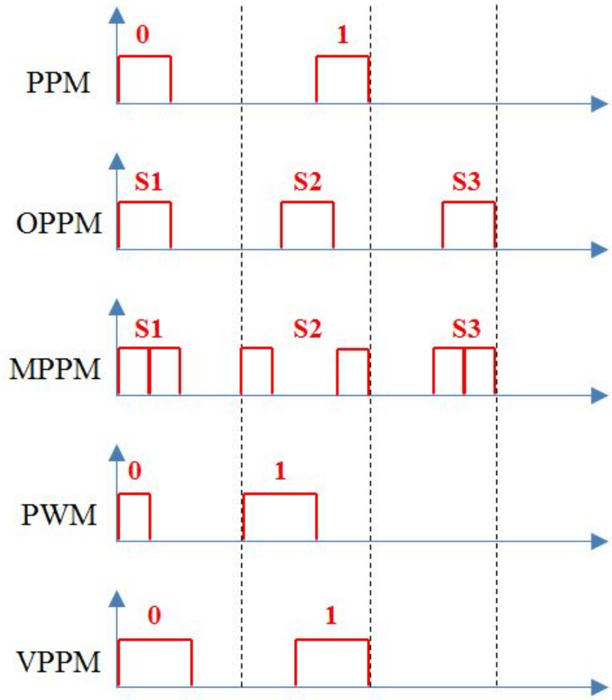

Figure 1.3: Schematic diagram for single carrier modulation techniques.

1.2.1.2 PPM

PPM is a pulse modulation technique based on the position of the pulse in the symbol period. In PPM, the symbol duration is divided into n equal slots and a pulse is transmitted in one of the n slots. The way of generating pulses in PPM is similar to OOK and the position of the pulse identifies the transmitted symbol.

Different PPM versions have been proposed over time to overcome the lower spectral efficiency and data rate limitations of PPM. Overlapping PPM (OPPM) allows transmitting more than one pulse during a symbol duration [11] and different pulse symbols overlap each other (see Fig. 1.3). [12] showed that OPPM can achieve a higher spectral efficiency and higher data rate compared to PPM. Another generalization of PPM is referred to as Multipulse PPM (MPPM) [13]. MPPM allows transmitting multiple pulses during the symbol duration, however, the pulses within a symbol duration do not have to be continuous. [11] show that MPPM can achieve a higher spectral efficiency compared to OPPM.

1.2.1.3 PWM

In PWM, the widths of the pulses are adjusted according to the desired level of dimming, while the pulses carry the modulated signal in a square waveform. PWM achieves the dimming without changing the intensity level of pulses. PWM provides various advantages such as requiring a lower peak transmit power, having a better spectral efficiency, and being more resistant to Inter-Symbol Interference (ISI) [14]. Providing a low data rate is the limitation of PWM.

In PWM and PPM, the input bits map on a symbol of fixed duration and both schemes require slot and symbol-level synchronization. IEEE 802.15.7 [15] proposes Variable PPM (VPPM) which is a hybrid of PPM and PWM. In VPPM, the bits are encoded by selecting different pulse positions as in PPM and the width of the pulse also can be modified. VPPM maintains the simplicity and robustness of PPM and allows different dimming levels by altering the pulse width [10].

1.2.1.4 PAM

In PAM, message information is encoded in the amplitude of the signal pulse. VLC can only use positive optical output power; therefore, only unipolar PAM can be implemented. PAM does not require complex circuits for both transmission and reception. The main advantage of PAM is its higher spectral efficiency with respect to the other binary-level modulations. On the other hand, PAM requires more power and large bandwidth for data transmission [16].

1.2.2 Multi-carrier

In multi-carrier modulation, instead of transmitting information through pulses, the information is encoded in subcarriers at different frequencies. Multi-carrier modulation offers higher data rates compared to single carrier modulation. At high data speeds, information signal is affected by ISI which limits the modulation bandwidth

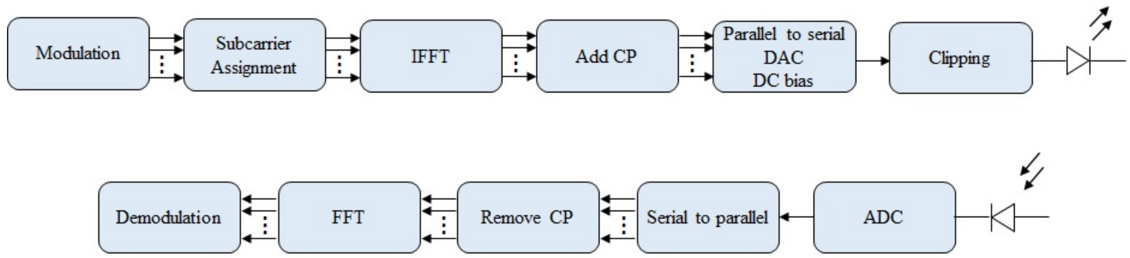

Figure 1.4: DCO-OFDM block diagram.

and communication rate [17]. Also, in the high frequency region, the channel frequency response is generally not flat. This requires the use of a complex equalizer in single carrier modulation [18]. Therefore, multi-carrier modulation, especially OFDM, is suitable in this scenario. OFDM enables simple equalization using single-tap equalizer in the frequency domain. In OFDM, the available bandwidth is divided into multiple narrowband subcarriers, which allow to adaptively allocate information bits and energy to individual subcarriers based on channel characteristics.

Conventional OFDM structure cannot be directly applied to the VLC systems, where the transmitted signals need to be real-valued and non-negative. In order to obtain the real-valued time domain signal, before the inverse fast Fourier transform (IFFT) Hermitian symmetry is needed to impose on the block of symbols. In order to obtain the non-negative time domain signals, DCO-OFDM and ACO-OFDM are widely used in typical VLC systems.

1.2.2.1 DCO-OFDM

In DCO-OFDM, a positive DC bias is added to make the time domain signal unipolar. The need for adding DC bias results in wasted transmission power. However, in the downlink DC bias is beneficial for providing illumination [19]. DCO-OFDM, is selected as the mandatory physical layer in IEEE standards on VLC, namely IEEE 802.15.13 [20] and IEEE 802.11bb [21]. In this thesis, we used this widely accepted and practical method as the basis of the physical layer (see Fig. 1.4).

At the transmitter side, the input bit stream is first mapped into complex symbols, i.e., $\mathrm{s}_1\ \mathrm{s}_2\ \cdots\ \mathrm{s}_{(K/2)-1}$, where K shows the number of subcarriers. Hermitian symmetry is then imposed on the data vector to ensure that the output of Inverse Discrete Fourier transform (IDFT) block is real.

The resulting data vector for the OFDM symbol transmitted from a LED at time t has the form of $\mathbf{X}(t) = \left[0\ \mathrm{s}_1\ \mathrm{s}_2\ \cdots\ \mathrm{s}_{(K/2)-1}\ 0\ \cdots\ \mathrm{s}^*_{(K/2)-1}\ \cdots\ \mathrm{s}^*_2\ \mathrm{s}^*_1\right]$. Afterwards, K-point IDFT is performed and a DC bias is added. Therefore, the transmitted waveform can be written as [19]

$$x_n(t) = \sum_{k=0}^{K-1} \underbrace{\frac{1}{\sqrt{K}} X^k(t) e^{j\frac{2\pi k}{K}n}}_{x_n^k(t)} + x_{DC}, \quad n = 0,\ 1,\ \dots,\ K-1, \tag{1.4}$$

where $X^k(t)$ is the k^{th} subcarrier of signal $\mathbf{X}(t)$ and x_{DC} is the DC bias. $x_n^k(t)$ denotes the n^{th} time-domain sample of the OFDM symbol transmitted from the LED on subcarrier k.

1.2.2.2 ACO-OFDM

ACO-OFDM is proposed to have an energy efficient unipolar OFDM signal. In ACO-OFDM, the information bits are carried only on odd-indexed subcarriers without adding DC bias and the even indexed subcarriers are set to zeros [19]. After K-point IFFT, the time domain signal satisfies

$$x\left(n + \tfrac{K}{2}\right) = -x\left(n\right) \quad n = 0, \cdots, \tfrac{K}{2} - 1. \tag{1.5}$$

The transmitted signal in an ACO-OFDM system can be expressed as

$$s(n) = \begin{cases} x(n) & x(n) > 0 \\ 0 & x(n) \leq 0 \end{cases} \tag{1.6}$$

ACO-OFDM sacrifices half of the spectral efficiency but it is more energy efficient compared to DCO-OFDM. In ACO-OFDM, only $K/4$ data symbols; therefore, the data rate of ACO-OFDM is given by [22]

$$R_{ACO-OFDM} = \left[\frac{K/4}{K + K_{CP}}\right] B \log_2(M), \tag{1.7}$$

where B is the bandwidth, K_{CP} is the length of cyclic prefix and M is the constellation size for Quadrature Amplitude Modulation (QAM) or Phase-Shift Keying (PSK) modulation scheme.

1.3 Literature Review

A tremendous growth in the number of mobile communication terminals has resulted in an ever-increasing demand for high-speed wireless data traffic in local area networks [23]. Current wireless access systems mostly work in the Radio Frequency (RF) band. However, this frequency band is almost wholly occupied and heavily regulated. In an effort to yield more bandwidth, ongoing research efforts focus on the upper segments of the RF band with a particular emphasis on millimeter-wave frequencies [24]. An alternative approach is the utilization of optical bands for wireless access. VLC builds upon the dual use of illumination infrastructure for wireless communication purposes [25]. In VLC systems, light from LEDs is modulated at high speeds without any adverse effects on illumination levels. Therefore, low cost and energy efficient LEDs already deployed in indoor environments can be utilized as Access Points (APs) to provide wireless access to multiple users as an add-on service to the primary task of illumination.

There has been a growing literature on VLC, see e.g., surveys [10,26,27] and references therein. Initial works have mostly focused on point-to-point VLC systems and addressed physical layer design issues. Some recent works [28–31] consider a cellular VLC network, where each LED serves as an AP and address upper layer issues in the downlink of multiuser VLC networks [32, 33]. Furthermore, some resource management studies including resource allocation, scheduling and interference management were reported in [34–40]. In [34], the scheduling problem for indoor multiuser VLC systems is investigated to minimize inter-user interference. In [35], resource allocation problem for a VLC system is formulated to achieve proportional fairness under delay requirements. In [36], a centralized resource allocation scheme is proposed to assign the visible light multicolor logical channels to different users to minimize the co-channel interference. In [37], a location-based proportional fair scheduling algorithm for VLC is introduced. An underlying assumption in [36] and [37] is that the users are always connected to the AP with the best channel information, therefore this does not guarantee that each user gets the best service. In [38], a centralized resource allocation method for a Orthogonal Frequency Division Multiple Access (OFDMA) based VLC system is proposed based on genetic algorithms to maximize system throughput. In [39], based on collision monitoring, a decentralized resource allocation method is introduced for OFDMA VLC system. In the proposed system of [39], each AP is required to broadcast the information of utilized resources.

Unlike the aforementioned studies [34–39], where traffic type and data rate requirements of the users are not considered, the work in [40] considers user satisfaction and addresses both resource allocation and load balancing for an OFDM VLC system, however, the proposed method does not consider the mobility of the user. Furthermore, there are some other studies to investigate resource allocation and load balancing in hybrid VLC - RF networks [41–44].

To support multiple users in a VLC network, various multiple access techniques were investigated including Time Division Multiple Access (TDMA) [45], Optical Code Division Multiple Access (OCDMA) [46], Space Division Multiple Access (SDMA) [47] and OFDMA [48]. In TDMA, each user is assigned certain time slots to maintain orthogonality. However, given the small coverage area of each VLC cell (also known as attocells [49]), TDMA is not a favorable option, because it suffers from inter-cell interference in overlapping coverage areas of APs and requires accurate synchronization between users and APs [50]. OCDMA builds upon the assignment of orthogonal optical codes to users to enable simultaneous transmission over the same frequency channel. However, in practice, it is difficult to generate orthogonal codes or codes with low cross-correlation for a large number of users. In SDMA, users are separated in the space domain by using multiple directional beams at the transmitter which requires custom-design LEDs or optics and introduces high implementation complexity.

Among these options, OFDMA stands out with features such as better spectral efficiency and low implementation complexity. It was also adopted in the IEEE 802.15.13 and IEEE 802.11bb standards under preparation [20]. This has prompted several researchers to investigate resource management issues for the performance optimization of OFDMA-based VLC networks. For example, in [51], Hammouda et al. proposed a resource allocation method to suppress the inter-cell interference based on a certain geometrical design of the cell area. In particular, they divided the coverage area into two location-based priority zones and proposed a two-step (i.e., cell-level and user-level) resource allocation scheme to allocate bandwidth and power resources. In [52], Ling et al. investigated the joint subcarrier assignment, power allocation and DC-bias optimization for an OFDMA-based multi-user VLC system.

As discussed above, there is a growing interest in OFDM-based VLC networks; however, these works only consider the short term optimization of system resources without the awareness of long term network operation constraints and objectives. Moreover, they do not consider the stochastic traffic arrivals. However, in practice, users have different types of data traffic, i.e., high-quality video streaming, voice, video telephony, online gaming, webcast, etc. For example, they might have delay-sensitive services with varying data arrivals. This requires the cross-layer design of VLC systems to cope with the stochastic traffic arrival rates and long term system constraints. While there were some efforts in the cross-layer design of hybrid RF/VLC systems [53–55], to the best of our knowledge, no prior work addressed the resource allocation problem in OFDM-based VLC networks from a cross-layer design perspective.

Another critical issue is handover that facilitates the transfer of a mobile user from one AP to another without causing any disruption in the existing session. Note that, in this thesis we consider horizontal (intra-system) handover. This differs from vertical handover which takes place between different access technologies. Vertical handover in hybrid VLC-RF networks has been already investigated in [56, 57]. Handover schemes can be categorized as "hard" or "soft" based on the number of simultaneous connections. Hard handover is a break-before-make method, where the connection to the current AP is broken before the connection to another AP is made. On the other hand, soft handover is a make-before-break method, where the connection to another AP is established before the connection to the current one is broken. The existing works that investigate handover schemes in the context of VLC networks include [58–63]. Particularly, in [58], a handover method based on received signal intensity is investigated for two indoor VLC scenarios consisting of overlapping (uniform lighting) and non-overlapping (spotlighting) cases. In [59], a hard handover scheme is studied that uses predictive received signal strength to reduce handover delay and frequency. In [60], cell coverage areas are dynamically changed to perform handover while maintaining desired illuminance in the environment. In [61], handover hysteresis regions are investigated for VLC systems under the illumination and Signal to Noise Ratio (SNR) constraints. The work in [62] optimizes the LED footprint for maximizing the average user data rate taking into account the number of users, user mobility and the number of handovers. In [63], two soft handover algorithms are considered for VLC. In these algorithms, while the user is in the intersection area of two APs, the second AP starts serving the user using either the same or different frequency range that the first AP uses. All existing works on VLC handover use a simplified analytical channel model limited to LOS. The effects of the obstacles, reflections and the rotation of the detector are not taken into account.

Vehicular networking is an essential component of Intelligent Transportation Systems (ITS) and builds on the reliable and scalable implementation of Vehicle-to-Vehicle (V2V), Vehicle-to-Infrastructure (V2I) and Infrastructure-to-Vehicle (I2V) links [64]. The collected information from the neighboring cars and roadside infrastructure provides the driver with real-time information on traffic and road conditions including collisions, congestion, traffic signal violations, emergency brakes, etc. Besides such safety functionalities, potential in-vehicle applications have recently emerged such as high-speed Internet access and mobile commerce [65].

The current research activities and standardization efforts on vehicular networking mainly focus on RF technologies [66,67]. However, limited RF bands can quickly suffer from high interference levels when hundreds of vehicles located in the same vicinity try to communicate simultaneously. In such user-dense environments, channel congestion might result in longer delays and lower packet rates. To address such issues, VLC has been proposed as an alternative means for vehicular connectivity [68–70].

In particular, uniformly placed highway street lights provide the required infrastructure for the implementation of I2V communication network, where each of VLC-enabled street lights can be configured to serve as an access point. Potential applications of vehicular VLC include real-time information on traffic and road conditions including collisions, congestion, traffic signal violations, emergency brakes, etc. Besides such safety functionalities, potential in-vehicle applications have recently emerged such as high-speed Internet access and mobile commerce [71].

A critical issue in such an I2V network is the design of the handover process required for efficient mobility management particularly given the relatively small coverage area of each light. Vertical and horizontal handover were studied extensively in indoor VLC networks see e.g., [56, 72–77] and references therein. Handover schemes proposed for indoor mobile VLC scenarios (i.e., optimized for pedestrian speeds) might be perhaps applicable for outdoor VLC systems if the vehicle velocity is sufficiently small. However, in general, the fast movement will seriously degrade the performance of such a system and make the system non-functional. This prompted researchers to investigate custom-design handover solutions for vehicular VLC networks [78–81].

The need for efficient handover in vehicular VLC networks was emphasized in [78, 79] without explicit details on the type of handover techniques. In [80], Dang and Yoo considered a I2V network, where a number of consecutive street lights are grouped as a cell. Under the assumption of an on-board camera used as a receiver, they proposed an inter-cell handover technique. The handover is based on the estimated distance between the vehicle and each group of street lights and the required distance estimation is obtained through image processing techniques. In [81], N. Zhu et.al. considered a vehicular scenario, where individual street lights serve as APs. They assumed both cases of overlapping and non-overlapping coverages and calculated received signal powers based on the Lambertian source model. Based on received signal strengths, they proposed a soft handover algorithm as a function of signal detection threshold and signal drop threshold. This handover scheme relies on the knowledge about the vehicle velocity and its implementation requires the estimation and feedback of velocity information.

1.4 Motivation and Contributions

There has been a growing attention on VLC over the last few years. The existing works in the literature on point-to-point VLC systems are well established and especially the studies on physical layer aspects demonstrate the potential of VLC. However, to transform VLC to a multi-user, multi-cell, scalable, and fully networked wireless technology significant additional efforts are required on upper layer issues, including resource allocation and mobility management. The main objective of this dissertation is to develop resource allocation and mobility management techniques for indoor and vehicular VLC systems.

In the first part of this thesis, we present a unified resource allocation and mobility management algorithm based on PSO for indoor VLC networks. We consider a VLC network, where multiple LEDs serve as APs. A centralized controller collects channel state information, quality of service requirements of the users, and the overload status of the APs. Based on the available information, in each time interval, the controller decides which user is served by which AP and assigns subcarriers to the users with the objective of maximizing both the system throughput and user satisfaction. We formulate the resource allocation problem as a constrained nonlinear integer programming problem and solve it using meta-heuristic PSO. Through an extensive simulation study, the superiority of the proposed algorithm in terms of system throughput and user satisfaction over round robin, best channel quality information, and genetic algorithms is demonstrated.

In the second part of this thesis, we propose a cross-layer resource management mechanism for an indoor multiuser VLC access network. The physical layer builds upon DC-biased orthogonal frequency division multiple access. Channel state information at the physical layer serves as a performance indicator for better data rate opportunity while queue state information at medium access control layer provides the information about packet urgency. A packet based traffic arrival model is considered such that incoming packets with random inter arrival times join a separate queue dedicated to each user if the admission control accepts them, otherwise packets are dropped. We formulate and solve a stochastic cross-layer optimization problem to optimize the network resources under the constraints of queue stability and power to maximize the average system throughput. By using the Lyapunov optimization technique, we convert the long term time-average optimization problem into series of single time slot online problems. Then, we decompose the problem into independent sub problems and propose packet admission, resource (access point and subcarrier) allocation and power control solutions. We present simulation results to demonstrate the superiority of proposed scheme over existing solutions in the literature.

In the last part of this thesis, we investigate handover techniques for indoor and outdoor VLC networks. First, we consider an indoor cellular VLC network, where each ceiling luminary serves as an AP. The network is assumed to support CoMP transmission. The user is mainly served by an AP (i.e., luminary) from which he/she gets the strongest signal. When the user moves towards the cell edge, the received signal from the served AP drops. Based on the handover algorithm decision, a handover to another AP can take place or CoMP is initiated. In the case of CoMP, the user is jointly served by two coordinating APs that transmit the same information. We compare the performance of proposed joint transmission-handover algorithm with conventional hard handover and demonstrate significant performance gains in terms of user data rate. Then, we consider an outdoor scenario and propose a dynamic soft handover algorithm based on CoMP transmission. The proposed algorithm takes the rate of change in the received power as an input and accordingly revises the handover margin and time-to-trigger value without explicit information of the vehicle velocity. Our simulation results demonstrate that the proposed algorithm outperforms conventional CoMP and hard handover and maintains a stable signal quality regardless of vehicle velocity.

Some parts of this research have been published as listed below [38, 82–85]:

- **M. S. Demir**, and M. Uysal. "A cross-layer design for dynamic resource management of VLC networks." *IEEE Transactions on Communications*, vol. 69, no. 3, pp. 1858-1867, 2021.

- **M. S. Demir**, H. Eldeeb, and M. Uysal. "CoMP-based dynamic handover for vehicular VLC networks." *IEEE Communications Letters*, vol. 24, no. 9, pp.

2024-2028, 2020.

- **M. S. Demir**, M. S. Sadiq, and M. Uysal. “Unified resource allocation and mobility management technique using particle swarm optimization for VLC networks.” *IEEE Photonics Journal*, vol. 10, no. 6, pp. 1-9, 2018.

- **M. S. Demir**, F. Miramirkhani, and M. Uysal. “Handover in VLC networks with coordinated multipoint transmission.” in *IEEE International Black Sea Conference on Communications and Networking (BlackSeaCom)*, pp. 1-5, 2017.

- **M. S. Demir**, O. F. Gemici, and M. Uysal, “Genetic algorithm based resource allocation technique for VLC networks,” in *IEEE Signal Processing and Communications Applications Conference (SIU)*, pp. 1–4, 2017.

CHAPTER II

UNIFIED RESOURCE ALLOCATION AND MOBILITY MANAGEMENT TECHNIQUE USING PSO

In this chapter, we propose a unified resource allocation and mobility management algorithm for indoor VLC networks. A centralized controller collects channel state information, Quality of Service (QoS) requirements of the users and the overload status of the APs. Based on the available information, in each time interval, the controller first decides which user is served by which AP and then assigns subcarriers to the users to maximize the system throughput and user satisfaction. We formulate the resource allocation problem as a constrained nonlinear integer programming problem and solve it using the meta-heuristic Particle Swarm Optimization (PSO). The performance of the proposed scheme is compared with Round Robin (RR), best Channel Quality Information (CQI) and Genetic Algorithms (GA) in terms of system throughput and user satisfaction.

2.1 System Model

As illustrated in Fig. 2.1, we assume a Centralized Light Access Network (C-LiAN) [86], where multiple LEDs serve as APs. There is a centralized controller responsible for mobility management and resource allocation. This controller is a gateway that connects VLC network to the Internet. It is assumed to have Channel State Information (CSI) of the links between users and the APs. Users are assumed to be randomly located in the indoor environment and the Random Waypoint Model (RWP) in [87] is used to model the user mobility.

The physical layer builds upon DCO-OFDM. Either PSK or QAM can be used in

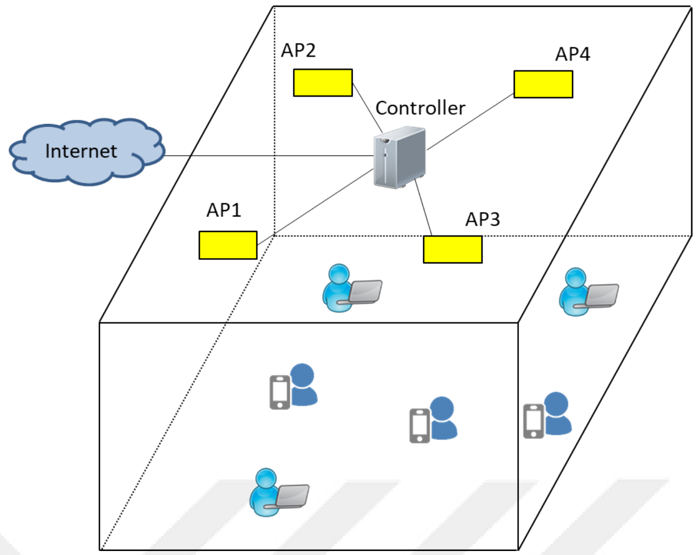

Figure 2.1: Indoor VLC network topology.

conjunction with DCO-OFDM system. We assume that there are N_{AP} APs serving a total of N users and an individual user can be served by only one AP. Each AP has K transmission channels (subcarriers) that are shared by a number of users. One or more subcarriers of an AP can be assigned to a specific user in each signaling interval.

At the receiver, the received signal by the u^{th} user, $1 < u \leq N$, on subcarrier k can be expressed as

$$y_{u,k}(t) = RH_{0,u}x_{0,k}(t) + R\sum_{i \in U} H_{i,u}x_{i,k}(t) + n_k(t), \tag{2.1}$$

where R is the responsivity of the photodetector and $n_k(t)$ denotes the noise signal with zero mean and variance of $\sigma_k^2 = N_0W/K$. Here, N_0 is the noise Power Spectral Density (PSD) and W is the total modulation bandwidth. In (2.1), $x_{i,k}(t)$ denotes the transmitted signal from the i^{th} AP on the k^{th} subcarrier. U denotes the set of interfering APs. Therefore, the first term of (2.1) represents the desired transmitted signal from AP serving the user and the second term denotes the received interference signal. Here, $H_{i,u}$ represents the channel coefficient between the i^{th} AP and the u^{th} user.

2.2 PSO Based Resource Allocation

In this section, we formulate a subcarrier allocation problem to maximize the user satisfaction index. In wireless networking, users have different types of data traffic (i.e., high-quality video, voice, delay sensitive data, etc) and therefore their data rate requirements vary. According to Jain's fairness index [88], satisfaction index for the overall network is defined as

$$\xi = \frac{(\sum_{u=1}^{N} \theta_u)^2}{N \sum_{u=1}^{N} \theta_u^2}. \tag{2.2}$$

Here, θ_u denotes the satisfaction degree of the i^{th} user and is given by [40]

$$\theta_u = \begin{cases} C_u/R_u, & \text{if } C_u < R_u \\ 1, & \text{otherwise} \end{cases} \tag{2.3}$$

where R_u denotes the required data rate and C_u represents the achievable data rate. Based on the ergodic channel capacity definition, C_u can be calculated as

$$C_u = \sum_{k=0}^{K-1} \sum_{i=0}^{N_{AP}-1} \alpha_{i,u}^{k} (W/K) \log_2(1 + \gamma_{u,k}), \tag{2.4}$$

where $\alpha_{i,u}^{k}$ represents a binary variable defined as

$$\alpha_{i,u}^{k} = \begin{cases} 1, & \text{if } k^{th} \text{ subcarrier of } i^{th} \text{ AP is assigned to the } u^{th} \text{ user} \\ 0, & \text{otherwise} \end{cases} \tag{2.5}$$

In (2.4), $\gamma_{u,k}$ denotes the Signal-to-Interference-Noise-Ratio (SINR) for the u^{th} user for subcarrier. Based on the signal model given by (2.1), it can be expressed as

$$\gamma_{u,k} = \frac{R^2 H_{0,u}^2 E_{0,k}}{R^2 \sum_{i \in U} H_{i,u}^2 E_{i,k} + \sigma_k^2}, \tag{2.6}$$

where $E_{i,k}$ denotes the transmitted electrical signal power from the i^{th} AP on subcarrier k. Noting that only $K-2$ subcarriers carry data and eta denotes the DC-bias factor which determines the level of DC-bias depth [89], $E_{i,k}$ is given by

$$E_{i,k} = \frac{\left(E\left[x_{i,k}(t)\right]\right)^2}{\eta^2 (K-2)}. \tag{2.7}$$

We formulate a subcarrier allocation problem to maximize the user satisfaction index. Mathematically speaking, we can express this optimization problem as

$$\text{maximize} \quad \xi = \frac{(\sum_{u=1}^{N} \theta_u)^2}{N \sum_{u=1}^{N} \theta_u^2} \tag{2.8}$$

$$\text{subject to} \quad \sum_{u=1}^{N} n_{i,u} \leq (K-2)/2, \quad 0 < i \leq N_{AP} - 1 \tag{2.9}$$

$$\sum_{i=0}^{N_{AP}-1} \alpha_{i,u}^{k} \leq 1, \quad 0 < k \leq K - 1, \tag{2.10}$$

where $n_{i,u}$ shows the number of assigned subcarriers of the i^{th} AP to the u^{th} user. The first constraint is imposed to guarantee that the sum of allocated subcarriers is smaller than the total number of available subcarriers. The second constraint guarantees that a subcarrier can be assigned to only one user.

This is a complicated constrained nonlinear integer programming problem. For such complicated optimization problems, an effective and accurate optimization method is needed; however, for nonlinear integer programming problems there is no known polynomial time algorithm to find the optimal solution [90]. PSO method proposed by Kennedy et al. [91] has drawn attention as one of the promising optimization methods with high speed and accuracy [92, 93]. PSO is a bio-inspired optimization algorithm motivated from the social dynamics of birds and fishes, where group of birds and fishes flock, change direction and move together in synchronization. Individuals called "particles" benefit from their own experiences and those of the other members of the swarm during the movement.

As illustrated in Fig. 2.2, in PSO, every particle has a velocity and a position which represents a candidate solution for a given optimization problem. At each iteration, a fitness function (i.e., objective function of optimization problem) is used to evaluate the solutions and each particle in the swarm moves toward to the historical personal

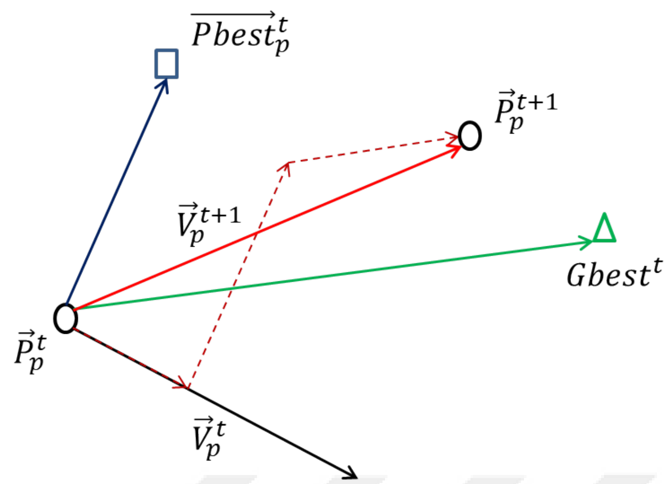

Figure 2.2: Movement of a particle.

best position and the global best position according to the set of equations given by [90]

$$V_p^{t+1} = wV_p^t + c_1(Pbest_p^t - P_p^t) + c_2(Gbest^t - P_p^t) \tag{2.11}$$

$$P_p^{t+1} = P_p^t + V_p^{t+1}, \tag{2.12}$$

at the t^{th} iteration, $1 < t \leq t_n$, where t_n is the PSO iteration number. In (2.11) and (2.12), ${P_p}^{\text{t}}$ represents the position of the p^{th} particle, $1 < p \leq p_n$, where p_n is the number of particles in the swarm. ${V_p}^{\text{t}}$ shows the velocity of the p^{th} particle at the t^{th} iteration. ${Pbest_p}^{\text{t}}$ represents the personal best position and $Gbest^{\text{t}}$ is the swarm's best position at the t^{th} iteration. w is the inertia term and c_1 and c_2 are the acceleration coefficients. At the end of the last iteration, $Gbest^{t_n}$ becomes the final PSO solution. In our case, $Gbest^{t_n}$ is a $K \times N_{AP}$ matrix with each element denoted as $Gbest^{t_n}(k,i) = u$ indicating that the k^{th} subcarrier of the i^{th} AP is assigned to the u^{th} user, i.e., $\alpha_{i,u}^k = 1$ in (2.10).

The pseudo code of proposed algorithm is described in Algortihm 2.1. Fig. 2.3 shows a sample PSO algorithm solution, $Gbest^{t_n}$, which represents a resource allocation map. For instance, as shown in the figure, 2^{nd} and 3^{rd} subcarriers of the 4^{th} AP is assigned to the 9^{th} user.

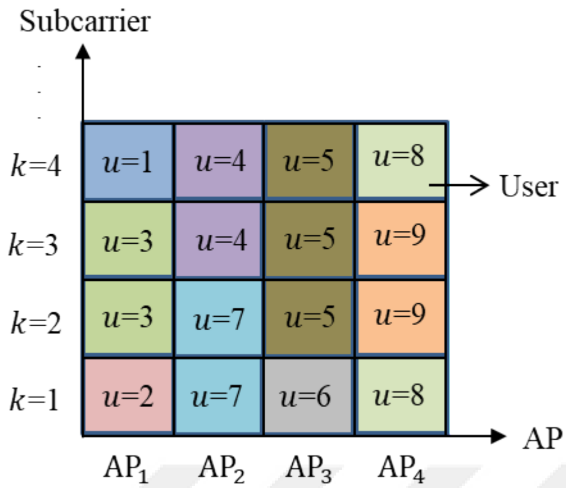

Figure 2.3: Allocation map.

Algorithm 2.1 Pseudo-Code of the Proposed Algorithm.

for each particle ($p = 1$ to p_n) **do**
    initialize random position (P_p^0) and velocity (V_p^0);
    eveluate fitness function ($Pbest_p^0$);
end for
compute global best position ($Gbest^0$);
for each iteration ($t = 1$ to t_n) **do**
    for each particle ($p = 1$ to p_n) **do**
        update position (P_p^t) and velocity (V_p^t);
        eveluate fitness function ($Pbest_p^t$);
    end for
    update global best position ($Gbest^t$);
end for
return global best position ($Gbest^{t_n}$);

Proposed algorithm is executed in each time interval considering the location and the data rate requirements of the users and the overload status of the APs. In each time interval, the algorithm decides which AP will serve a specific user and which subcarriers of that AP will be assigned to that user. If there are overloaded APs, the controller performs load balancing and handovers to transfer the users to the neighboring available APs. It should be noted that this is imposed by the first constraint in (2.8). This constraint ensures that the algorithm does not allocate more subcarriers beyond the AP capacity. Furthermore, based on the channel condition (mainly determined by the location) of the user checked at every signaling interval on a regular basis, the controller handovers the user to available AP with a better channel state, if required.

2.3 Simulation Results and Discussions

In this chapter, we consider an empty room with a size of 5 m $\times$ 5 m $\times$ 3 m and assume 4 luminaries (each acting as an AP) on the ceiling with equidistant spacing of 2.5 m in both x and y directions. The optical power for each luminary is 55 Watts and they have 40° half viewing angle. The height of the photodetectors are 0.75 m and they face upward towards the ceiling. The FOV and the area of the PDs are 85° and 1 cm^2, respectively. The number of users varies from 6 to 22 and the number of subcarriers for each AP is 16. As stated in Section 2.1, RWP is used to model the user mobility. At the beginning of each trip, the mobile user chooses a random destination and a speed. Then, it travels toward the new destination at a constant speed of 3 km/h. Simulation parameters are summarized in Table 2.1.

Table 2.1: Configuration parameters.

Parameters	**Values**
Size of room (L $\times$ W $\times$ H)	5 m $\times$ 5 m $\times$ 3 m
Number of luminary	4
Power of each luminary	55 W
View angle of luminary	40°
Distance between luminaries	2.5 m
FOV of PD	85°
Area of PD	1 cm^2
Responsivity of PD	0.6 A/W
Vertical separation of transmitter and receiver	2.25 m
Noise density	1×10^{-20} A^2/Hz
AP signal bandwidth	20 MHz
DC bias factor	3
Number of subcarrier	16

In Fig. 2.4, we present the system throughput with respect to the number of users. The number of particles in the swarm p_n is 30, and the number of PSO iteration t_n is set to 70. Constant part of the acceleration coefficients c_1 and c_2 are set to 2.5 and inertia term w is chosen as 0.5. As benchmarks, we include the performance of RR algorithm [37], best CQI [40] and GA [38, 94]. RR aims to equally allocate the resources among users to provide fairness. CQI algorithm is designed to give priority to the user having strongest channel condition. GA is a population based iterative heuristic algorithm and aims to find an optimal solution for a defined problem.

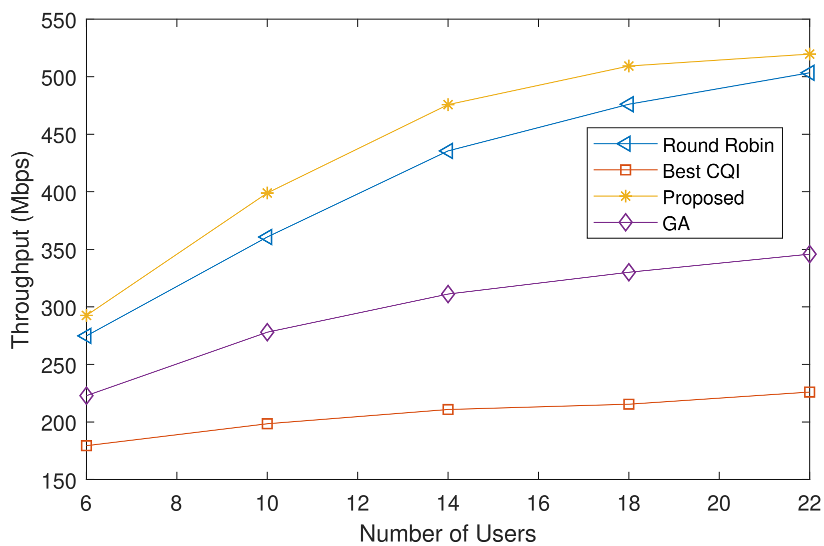

Figure 2.4: System throughput versus the number of users.

From Fig. 2.4, we observe that our proposed algorithm outperforms RR, best CQI and GA techniques. For example, when the number of users is set to 14, our algorithm provides a total system throughput of 476 Mbps while RR, GA and best CQI provide 436 Mbps, 311 Mbps and 210 Mbps, respectively. Best CQI algorithm tries to give all the resources to the user that has the best channel information and it does not consider the user's required data rate, therefore it has the worst throughput performance. GA approach has the second worst performance; in our simulation for a fair comparison, we set equal iteration numbers (i.e., 70) for both PSO and GA. It is observed that GA has poor performance, because it requires high iteration numbers to find an optimal solution. RR algorithm gives relatively better results compared to GA and best CQI. However, it does not consider the overload status of the APs, thus its throughput performance is worse than our proposed algorithm.

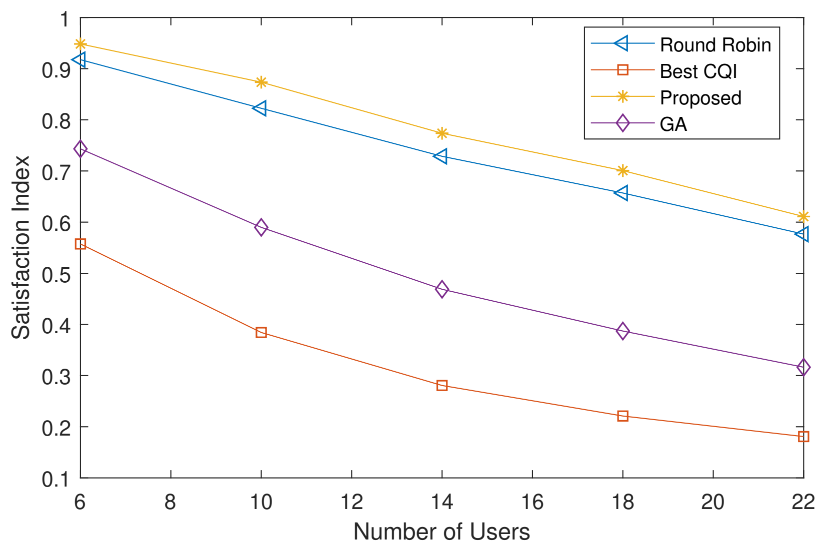

Figure 2.5: User satisfaction versus the number of users.

Fig. 2.5 presents the satisfaction index as a fairness indicator. Our algorithm achieves better performance in terms of fairness. For 14 users, our satisfaction index is 0.78 while RR, GA, and best CQI have satisfaction index of 0.73, 0.47 and 0.28, respectively. RR algorithm equally allocates the subcarriers, however it does not consider the user's required data rate and therefore it ends up with worse fairness. As expected, where there are limited resources, satisfaction index decreases when the number of user increases.

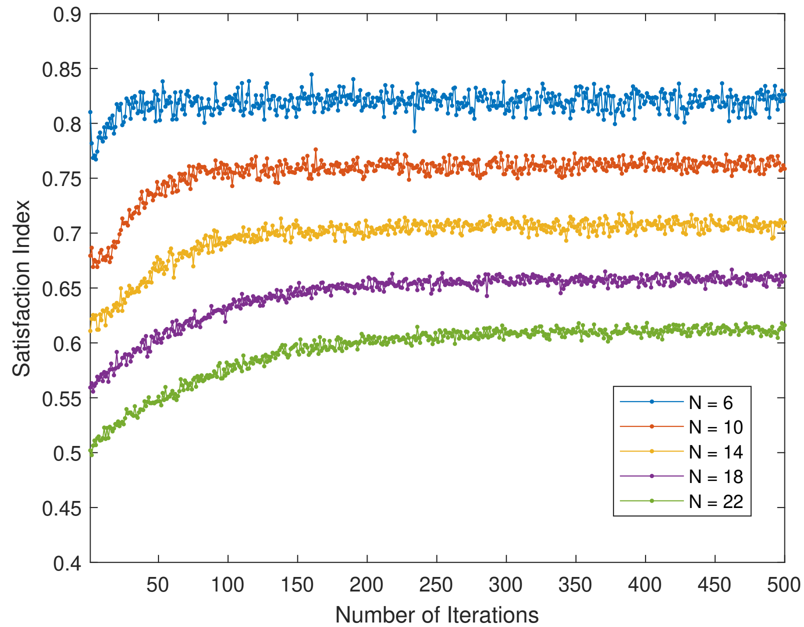

Figure 2.6: User satisfaction versus the number iterations.

Fig. 2.6 shows the user satisfaction index of the proposed algorithm as a function of the number of iterations. For $N = 6$ users, the proposed algorithm reaches a saturation point after about 50 iterations. The number of iterations required for convergence increases with the number of users. For example, it climbs to about 80, 130, 170 and 240 for $N = 10$, 14, 18 and 22.

CHAPTER III

A CROSS-LAYER DESIGN FOR DYNAMIC RESOURCE MANAGEMENT

In this chapter, we propose a cross-layer resource management mechanism for an OFDMA-based indoor multiuser VLC access network. We assume that there is a centralized control unit (CU) responsible for data admission, resource (AP and sub-carrier) allocation, and power control. The CU allows an interaction between physical (PHY) and medium access control (MAC) layer. CSI at the PHY layer serves as a performance indicator for better data rate opportunity while queue state information (QSI) at MAC layer provides the information about packet urgency. In the proposed mechanism, a packet based traffic arrival model is considered such that incoming packets with random inter arrival times join a separate queue dedicated to each user if the admission control accepts them, otherwise packets are dropped. Based on CSI and QSI, the CU aims to maximize the long term time-averaged system throughput while guaranteeing queue stability to avoid network congestion. By using the Lyapunov optimization framework, we convert this long term optimization problem into a series of single time slot online sub-problems. Then we solve each of these sub-problems including admission control, resource allocation and power control. Simulation results show that our technique provides an improved system performance while satisfying the system constraints.

3.1 System Model

As shown in Fig. 3.1, we consider the downlink of a centralized multiuser VLC-based access network, where M ceiling LEDs serve as APs in addition to their illumination

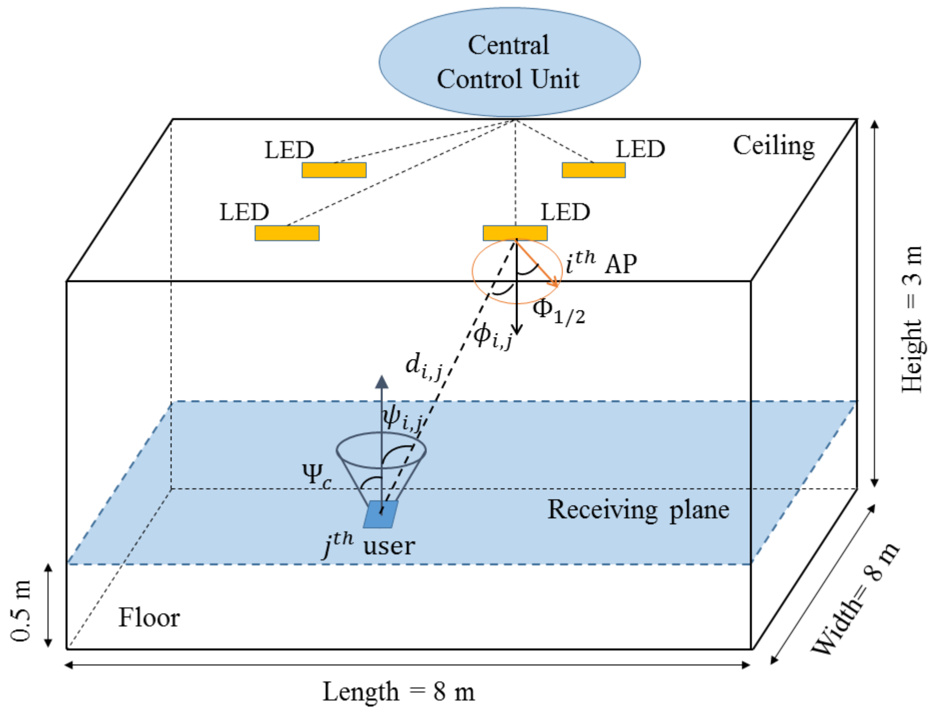

Figure 3.1: Indoor VLC network.

purpose. The CU is responsible for data admission, resource allocation and power control as well as acts as a gateway that connects VLC network to the Internet. As illustrated in Fig. 1.4, we employ DC-biased OFDMA (DCO-OFDMA), where M APs serve a total of N users. There is a total of $M \times K$ subcarriers and each AP is allocated K orthogonal subcarriers. Among these, only $K/2 - 1$ subcarriers per AP are used for data transmission due to Hermitian symmetry imposed in DCO-OFDMA [95]. It is assumed that an individual user can be served by only one AP. The minimum resource allocation unit that the serving AP can assign to a specific user consists of a single subcarrier with a duration of T_s and a single timeslot which contains multiple OFDM symbols.

Since ceiling LEDs (acting simultaneously as APs) have overlapping illumination areas, it is inevitable that users can receive signals from multiple APs. Since users associated with different APs might be assigned to the subcarriers using the same frequency, interference might occur. In the presence of interference, it is critical to allocate the proper AP and subcarriers for each user and adjust the transmit power of APs. In each time slot, this allocation decision is made by the CU using resource allocation algorithms designed to maximize the average system throughput (see Section 3.3 for further details on our algorithms). The CU makes this decision based on the QSI as well as CSI which is made available by a feedback through uplink channel. In practice, channel estimation can be performed by using pilot signals into the transmitted frame known by the receiver. Indoor VLC channel is a fading-free (deterministic) channel due to inherent aperture averaging [96] and exhibits only small variations due to the user's mobility and orientation. Therefore, channel estimation can be easily performed by using few pilot signals resulting in a small spectral efficiency loss. In our paper, we assume perfect CSI and ideal feedback channel. The transmission of a real-valued channel coefficient requires infinite bits. However, as demonstrated in [97], a few quantization bits are sufficient to provide a performance close to the ideal case. Therefore, feedback bits can be easily added without much burden on the uplink capacity.

Let $P_i(t)$ denote the optical transmit power of the i^{th} AP. Illumination constraints dictate a minimum optical power constraint $P_{\min} \leq P_i(t)$. On the other hand, in order to prevent from clipping noise, there is a maximum instantaneous power constraint $P_i(t) \leq P_{\max}$. For energy consumption concerns, the average power of the signal is further restricted as

$$P_i = \lim_{T\rightarrow\infty} \frac{1}{T} \sum_{t=0}^{T-1} \mathbb{E}\left[P_i(t)\right] \leq P_{\mathrm{av}}, \quad \forall i \ \in I, \tag{3.1}$$

where $I \triangleq \{1, \cdots, M\}$ shows the set of APs, $\mathbb{E}[.]$ represents the expectation operator, T shows the number of time slots and P_{av} is the maximum average power.

At the receiver, the received signal by the j^{th} user from the i^{th} AP on subcarrier k of the o^{th} OFDM symbol at time slot t can be expressed as [98]

$$y_j^{o,n,k}(t) = R\frac{P_i(t)}{\sqrt{(K-2)}\eta} G_{i,j}(t) x_i^{o,n,k}(t) + R\sum_{l\in D} \frac{P_l(t)}{\sqrt{(K-2)}\eta} G_{l,j}(t) x_l^{o,n,k}(t) + n_j^k, \ 1 < j \leq N, \tag{3.2}$$

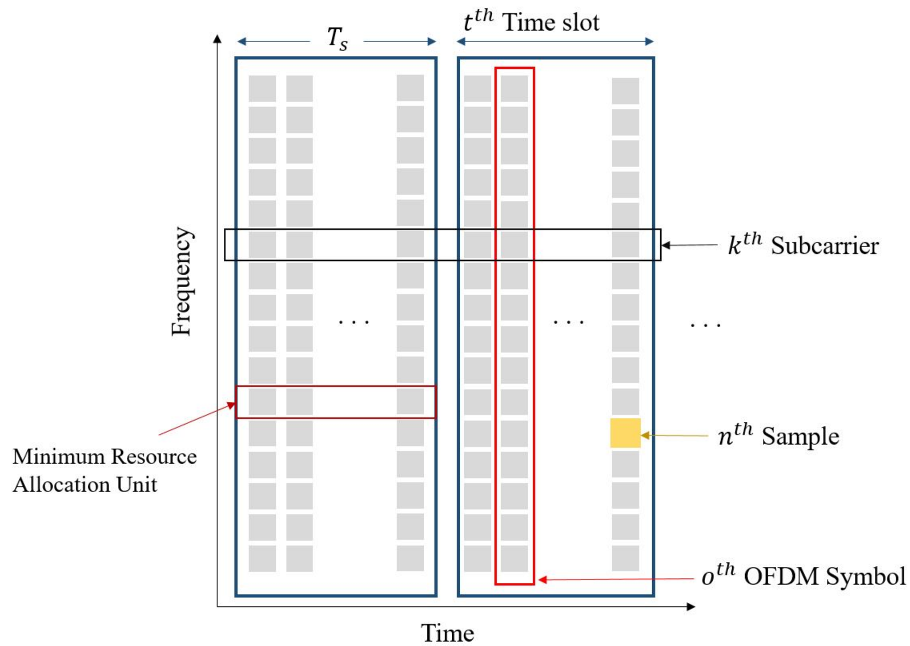

Figure 3.2: Minimum resource allocation unit.

where $x_i^{o,n,k}(t)$ denotes the n^{th} time-domain sample of the o^{th} OFDM symbol transmitted from the i^{th} AP on subcarrier k. Here, η is electrical-to-optical conversion ratio, R is the responsivity of the photodetector and D denotes the set of interfering APs. In (3.2), n_j^k is the noise term with zero mean and variance of $\sigma_k^2 = N_0W/K$. Here, N_0 is the noise PSD and W is the total modulation bandwidth. $G_{i,j}(t)$ denotes the optical channel coefficient between the i^{th} AP and the j^{th} user at time slot t.

Based on (3.2), the signal-to-interference-noise-ratio (SINR) for the j^{th} user on subcarrier k can be expressed as

$$\gamma_{i,j}^k(t) = \frac{R^2 P_i^2(t) G_{i,j}^2(t)}{R^2 \sum\limits_{l \in D} P_l^2(t) G_{l,j}^2(t) + (K-2)\eta^2\sigma_k^2}. \tag{3.3}$$

In VLC systems, the information is transmitted by modulating the instantaneous optical intensity and the signals are restricted to be positive. Although the exact capacity of the VLC channel remains unknown, the achievable data rate of the j^{th} user can be approximated as [99]

$$C_j(t) = \sum_{k=1}^{K} \sum_{i=1}^{M} \frac{\alpha_{i,j}^k(t)}{2\ln(2)} \frac{W}{K} \ln\left(1 + \frac{\exp(1)\gamma_{i,j}^k(t)}{2\pi}\right), \tag{3.4}$$

where $\alpha_{i,j}^k(t)$ represents a binary variable defined as

$$\alpha_{i,j}^k(t) = \begin{cases} 1, & \text{if } k^{th} \text{ subcarrier of } i^{th}\text{AP is assigned to the } j^{th} \text{ user at time } t \\ 0, & \text{otherwise} \end{cases} \tag{3.5}$$

3.2 Cross-layer Optimization Problem

As illustrated in Fig. 3.3, we consider a cross-layer design for resource management. Let $Q_j(t)$ denote the number of packets waiting in the queue at the beginning of timeslot t for the j^{th} user. Let $\lambda_j(t)$ represent the number of packet arrivals for the j^{th} user's queue at time slot t. Furthermore, let $\mu_j(t)$ and $f_j(t)$ represent the number of delivered and dropped packets associated with the j^{th} user. Therefore, the current queue backlogs vector, the packet arrival vector, the packet departure vector and the dropped packet vector can be then written respectively as $\mathbf{Q}(t) = (Q_1(t), \ \ldots, \ Q_N(t))$, $\lambda(t) = (\lambda_1(t), \ \ldots, \ \lambda_N(t))$, $\mu(t) = (\mu_1(t), \ \ldots, \ \mu_N(t))$ and $\mathbf{f}(t) = (f_1(t), \ \ldots, \ f_N(t))$. $\lambda_j(t)$ has a Poisson distribution with an average of λ_j and there exists a constant upper bound $\lambda_{\max}$ on data arrivals such that $\lambda_j(t) \leq \lambda_{\max}$. Similarly, we have $\mu_j(t) \leq \mu_{\max}$. Based on the above definitions, discrete-time queue dynamics of arrival and departure processes at the CU can be expressed as

$$Q_j(t+1) \leq \max\left[Q_j(t) - \mu_j(t), 0\right] - f_j(t) + \lambda_j(t), \quad \forall j \ \in J, \tag{3.6}$$

where $J \triangleq \{1, \cdots, N\}$ shows the set of users. The average queue backlog of the j^{th} user can be calculated as

$$Q_j = \lim_{T\to\infty} \frac{1}{T} \sum_{t=0}^{T-1} \mathbb{E}\left[Q_j\left(t\right)\right]. \tag{3.7}$$

A queue is defined as stable [100] if the long term departure rate is equal to the long term arrival rate, then the time average of the arrival process must be less than

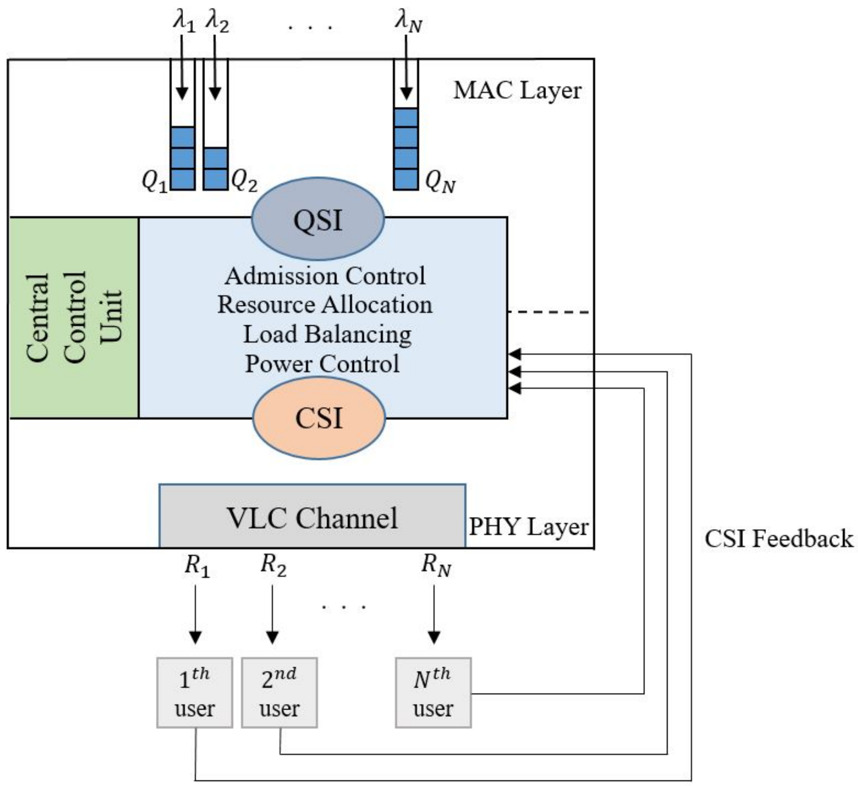

Figure 3.3: Cross-layer design concept for resource management.

or equal to the departure rate. A queue is defined as strongly stable if its backlog is always finite on average, $Q_j < \infty \ , \quad \forall j \ \in J$. A network is strongly stable if all individual queues in the system are strongly stable [100]. The total system throughput can be further defined as [101]

$$U(t) = \sum_{j \in J} \lambda_j(t) - f_j(t). \tag{3.8}$$

Our objective is to maximize the average system throughput function under a number of constraints expressed as follows

$$\text{maximize} \quad \lim_{T\to\infty} \frac{1}{T}\sum_{t=0}^{T-1} U(t) \tag{3.9}$$

$$\text{subject to} \quad P_{\min} \leq P_i(t) \leq P_{\max}, \quad \forall i \in I \tag{3.9a}$$

$$P_i \leq P_{\text{av}}, \quad \forall i \in I \tag{3.9b}$$

$$Q_j < \infty, \quad \forall j \in J \tag{3.9c}$$

$$\mu_j(t) \leq Z_j(t), \ \forall j \in J \tag{3.9d}$$

$$f_j(t) \leq \lambda_j(t), \ \forall j \in J. \tag{3.9e}$$

Here, $Z_j(t) = \lfloor C_j(t)T_s/S \rfloor$, where S denotes the packet size in bits to represent the maximum number of packets that can be transferred to the j^{th} user at time slot t. (3.9a) and (3.9b) ensure the maximum instantaneous and average power constraints of each APs, respectively. Constraint (3.9c) ensures the queue stability of the j^{th} user. Constraint (3.9d) shows that the number of departure packets cannot exceed the link capacity at any time t. Constraint (3.9e) implies that the number of dropped packets cannot be greater than the number of arrived packets at any time t.

The solution to the stochastic optimization problem in (3.9) requires the statistical knowledge about future CSI and data packets. Since it is not practical to make such idealistic assumptions, we resort to Lyapunov optimization technique [53, 102] which does not require prior knowledge. Lyapunov optimization defines a drift plus penalty term and makes online decisions which depend on the current state to solve the network utility optimization problem by minimizing the drift and penalty term. To solve (3.9), we first transform the long-term power constraint (3.9b) into a queue stability problem. We define a virtual queue vector $\mathbf{Y}(t) = (Y_1(t), \ \ldots, \ Y_M(t))$, where each virtual queue has the following queue dynamics:

$$Y_i(t+1) \leq \max\left[Y_i(t) - P_{\text{av}}, 0\right] + P_i(t), \quad \forall i \in I. \tag{3.10}$$

As described earlier, $P_i(t)$ and P_{av} respectively denote the optical transmit power of the i^{th} AP and the maximum average power of AP. Note that $Y_i(t)$ does not stand for any real queue or data; therefore, we call it virtual queue and it is only generated by the proposed algorithm. In the context of virtual queues, $P_i(t)$ can be intuitively viewed as the arrival rate of the virtual queue $Y_i(t)$, while P_{av} can be viewed as the departure rate. If the backlog in the virtual queue is stabilized, the time-average arrival rate (corresponding to $P_i(t)$) cannot be larger than the departure rate (corresponding to P_{av}). Therefore, the average power constraint in (3.9b) can be transformed into a single queue stability problem and stabilizing the virtual queue vector ensures the satisfaction of the desired average power constraint in (3.9b).

Then, we define Lyapunov function which is a non-negative function of all queues in the network as well as Lyapunov drift which is used to obtain control algorithms for the stability of the network. These control algorithms give decisions in order to minimize the Lyapunov function from one slot to the next. Let $\mathbf{\Theta}(t) = [\mathbf{Y}(t), \mathbf{Q}(t)]$ as the matrix of all virtual and real queues. We define a quadratic Lyapunov function as a scalar metric of aggregate congestion of all queues

$$L(\mathbf{\Theta}(t)) = \frac{1}{2}\sum_{i\in I} {Y_i}^2(t) + \frac{1}{2}\sum_{j\in J} {Q_j}^2(t). \tag{3.11}$$

Lyapunov drift defines the expected difference in the Lyapunov function over one slot. One-slot conditional Lyapunov drift at time t is therefore given by

$$\Delta(\mathbf{\Theta}(t)) = \mathbb{E}\left[L(\mathbf{\Theta}(t+1)) - L(\mathbf{\Theta}(t))\,|\mathbf{\Theta}(t)\right]. \tag{3.12}$$

Theorem 1. *Lyapunov drift is bounded by*

$$\Delta(\mathbf{\Theta}(t)) \leq B - \mathbb{E}\left[H(t)\,|\mathbf{\Theta}(t)\right], \tag{3.13}$$

where B is a finite constant defined as

$$B = \frac{1}{2}M\left(P_{\max}^2 + P_{av}^2\right) + \frac{1}{2}N\left(2\lambda_{\max}^2 + \mu_{\max}^2\right) \tag{3.14}$$

and $H(t)$ is defined as

$$H(t) \triangleq \sum_{i\in I} Y_i(t)\left(P_i(t) - P_{av}\right) + \sum_{j\in J} Q_j(t)\left(\lambda_j(t) - f_j(t) - \mu_j(t)\right) - \lambda_j(t) f_j(t) \tag{3.15}$$

Proof. Recalling the equation (3.9) and squaring this equation, we obtain

$$Y_i(t+1)^2 - Y_i(t)^2 = (\max[Y_i(t) - P_{\text{av}}, 0] + P_i(t))^2 - Y_i(t)^2 \tag{3.16}$$

$$\leq (\max[Y_i(t) - P_{\text{av}}, 0])^2 + 2P_i(t)\max[Y_i(t) - P_{\text{av}}, 0] + P_i(t)^2 - Y_i(t)^2 \tag{3.17}$$

$$\leq P_{\max}^2 + P_{\text{av}}^2 + 2Y_i(t)(P_i(t) - P_{\text{av}}), \tag{3.18}$$

where in the final inequality we use the following facts: $P_i(t) \leq P_{\max}$, $\max[Y_i(t) - P_{\text{av}}, 0] \leq Y_i(t)$ and $(\max[Y_i(t) - P_{\text{av}}, 0])^2 \leq (Y_i(t) - P_{\text{av}})^2$.

Similarly, by recalling the equation (3.6), we obtain

$$Q_j(t+1)^2 - Q_j(t)^2 = (\max[Q_j(t) - \mu_j(t), 0] - f_j(t) + \lambda_j(t))^2 - Q_j(t)^2 \tag{3.19}$$

$$\leq 2\lambda_{\max}^2 + \mu_{\max}^2 + 2Q_j(t)(\lambda_j(t) - f_j(t) - \mu_j(t)) - 2\lambda_j(t) f_j(t). \tag{3.20}$$

Based on (3.12) and using (3.18) and (3.20), we have

$$\Delta(\boldsymbol{\Theta}(t)) = \mathbb{E}\left[\frac{1}{2}\sum_{i\in I} Y_i(t+1)^2 - Y_i(t)^2 + \frac{1}{2}\sum_{j\in J} Q_j(t+1)^2 - Q_j(t)^2 \,|\boldsymbol{\Theta}(t)\right] \tag{3.21}$$

$$\leq \mathbb{E}\Bigg[\frac{1}{2}\sum_{i\in I} P_{\max}^2 + P_{\text{av}}^2 + 2Y_i(t)(P_i(t) - P_{\text{av}}) + \frac{1}{2}\sum_{j\in J} 2\lambda_{\max}^2 + \mu_{\max}^2 + 2Q_j(t)(\lambda_j(t) - f_j(t) - \mu_j(t)) - 2\lambda_j(t) f_j(t) \,|\boldsymbol{\Theta}(t)\Bigg] \tag{3.22}$$

$$\leq \underbrace{\frac{1}{2}M\left(P_{\max}^2 + P_{\text{av}}^2\right) + \frac{1}{2}N\left(2\lambda_{\max}^2 + \mu_{\max}^2\right)}_{B} + \mathbb{E}\Bigg[\underbrace{\sum_{i\in I} Y_i(t)(P_i(t) - P_{\text{av}}) + \sum_{j\in J} Q_j(t)(\lambda_j(t) - f_j(t) - \mu_j(t)) - \lambda_j(t) f_j(t)}_{H(t)} \,|\boldsymbol{\Theta}(t)\Bigg] \tag{3.23}$$

$$\leq B - \mathbb{E}[H(t)\,|\boldsymbol{\Theta}(t)] \tag{3.24}$$

□

Since B is a constant minimizing the Lyapunov drift, (3.12) can be simplified by minimizing $\mathbb{E}[H(t)]$. In order to stabilize all queues while maximizing the system throughput function [100], we define the minimization problem of "drift-plus-penalty" as follows:

$$\underset{f_j(t),\mu_j(t),P_i(t)}{\text{minimize}} \quad \mathbb{E}[H(t) - VU(t)] \tag{3.25}$$

$$\text{subject to} \quad P_{\min} \leq P_i(t) \leq P_{\max}, \quad \forall i \in I \tag{3.25a}$$

$$\mu_j(t) \leq Z_j(t), \ \forall j \in J \tag{3.25b}$$

$$f_j(t) \leq \lambda_j(t), \ \forall j \in J. \tag{3.25c}$$

Here, non-negative parameter V controls the tradeoff between the system constraints and the maximization of the system throughput function. Based on the concept of opportunistically minimizing an expectation [100], packet admission control $\mathbf{f}(t)$, resource allocation action $\mu(t)$ and power control action $\mathbf{P}(t)$ can be decided to minimize the drift plus penalty term by observing $\mathbf{\Theta}(t)$ and $\mathbf{Q}(t)$. The reformulated optimization problem in (3.25) is a constrained mixed integer programming problem, where $f_j(t)$ and $\mu_j(t)$ takes integer values and $P_i(t)$ takes continuous values. Finding the global optimum solution for this mixed integer programming problem is NP-hard [103]. In the following section, we decompose the problem in (3.25) into three sub-problems and then solve each of them individually.

3.3 Design of Resource Management Algorithms

In this section, we decompose the NP-hard optimization problem in (3.25) into three sub-problems and propose separate algorithms for data admission, resource allocation, and power control.

3.3.1 Admission Control

In an effort to decompose the main problem, we first isolate $f_j(t)$ terms and remove terms that do not contain $f_j(t)$ in (3.25). Therefore, the optimization problem in

(3.25) reduces to

$$\begin{aligned} \underset{f_j(t)}{\text{maximize}} \quad & \sum_{j \in J} (Q_j(t) + \lambda_j(t) - V) f_j(t) && (3.26) \\ \text{subject to} \quad & f_j(t) \leq \lambda_j(t), \ \forall j \ \in J. && (3.26a) \end{aligned}$$

Optimal solution for the above admission control problem depends on the arrival rate $\lambda_j(t)$, queue backlog $Q_j(t)$ and the parameter V. The maximization yields the simple threshold based solution in the form of

$$f_j(t) = \begin{cases} \lambda_j(t), & \text{if } Q_j(t) > V - \lambda_j(t) \\ 0, & \text{otherwise} \end{cases} \tag{3.27}$$

According to (3.27) when the queue backlog $Q_j(t)$ is larger than the threshold $V - \lambda_j(t)$, all the newly arrived data will be rejected to ensure the queue stability. Given the same queue backlog and data arrival, a smaller value of V implies a tough admission control policy, rejecting more arriving data. On the other hand, a larger V allows admission control policy to admit more incoming data in an effort to improve system throughput; however, there is an upper bound for throughput since there are limited system resources. It should be emphasized that the admission control action is performed dynamically with the use of queue backlog information $Q_j(t)$ and packet arrival information $\lambda_j(t)$.

3.3.2 Resource (AP and Subcarrier) Allocation

After isolating $\mu_j(t)$ and removing other terms, we can rewrite (3.25) as

$$\begin{aligned} \underset{\mu_j(t)}{\text{maximize}} \quad & \sum_{j \in J} Q_j(t) \mu_j(t) && (3.28) \\ \text{subject to} \quad & \mu_j(t) \leq Z_j(t), \ \forall j \ \in J. && (3.28a) \end{aligned}$$

The optimum solution for the above objective function always achieves the equality in constraint (3.28a), $\mu_j(t) = Z_j(t)$. Therefore, optimum solution is obtained by finding the optimal resource allocation variable $\alpha_{i,j}^k(t)$ defined in (3.5). Recall that

$\alpha_{i,j}^{k}(t)$ shows the mapping of subcarriers of an AP to users. To determine the optimum user, AP and subcarrier selection at each time slot, one naive solution is to evaluate all possible combinations through the exhaustive search for this complicated constrained integer programming problem. In our case, there are M APs with K subcarriers serving N users which indicates that the search space has $N^{(M\times(K/2-1))}$ possible solutions. Therefore, such a brute-force method is computationally prohibitive for most practical purposes.

Here, we use GA, a bio-inspired population based meta-heuristic algorithm [104], to solve this problem in a computationally efficient way. GA technique is a very powerful heuristic for exploring prohibitively huge search spaces [105] and it can be successfully employed in real-time applications [106–108]. In the GA approach, the computational complexity mainly depends on the population size (initial solutions), the number of iterations and fitness function. Let N_{pop} and N_{it} respectively denote the initial population size and the maximum number of iterations. At each generation (iteration), the fitness function for candidate solutions is calculated as $N_{pop}\times 6$ times which is the maximum population size reached after the crossover and mutation operations. Therefore, the GA algorithm evaluates a total of $N_{pop}\times 6\times N_{it}$ candidate solutions, which is much smaller than the original search space of $N^{(M\times(K/2-1))}$ in most cases of interest. For example, in a scenario including 16 users, 4 APs, and 16 subcarriers, we will have $16^{4\times 7}\cong 5.19\times 10^{33}$ possible solutions. For this scenario, when initial population size is set as $N_{pop}=8$ and the number of GA iteration is set as $N_{it}=100$, GA compares $8\times 6\times 100=4800$ possible solutions which is a tiny fraction of 5.19×10^{33} possible solutions that exhaustive search method requires. For real-time implementation, it is essential that this reduced solution set should be searched within a time slot duration. FPGA implementation of the GA algorithm for most applications can achieve a sufficiently short execution time in the order of tens of microseconds [108]. Therefore, our proposed GA algorithm with modest requirements

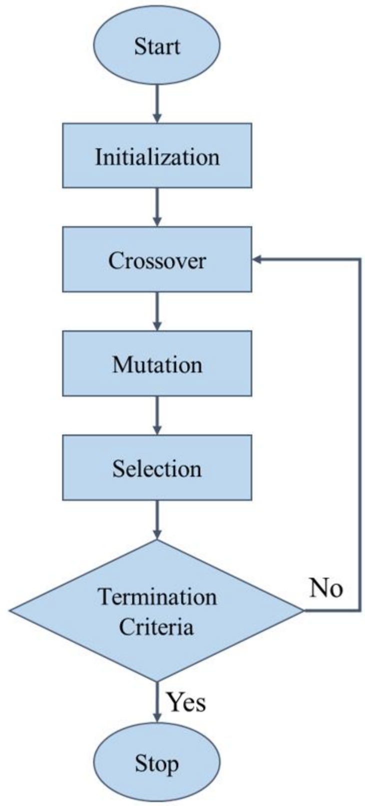

Figure 3.4: Flow chart of GA.

on the initial population size and the number of iterations, if implemented on an FPGA platform, could be executed in a duration less than the time slot duration.

The algorithm flowchart is shown in Fig. 3.4. Our algorithm tries to find $\alpha_{i,j}^{k}(t)$ by observing the queue backlogs of $Q_j(t)$ in every time slot. First we initiate a certain number of individuals (i.e., chromosomes that represents $\alpha_{i,j}^{k}(t)$) in the population as a subset of $N^{(M\times(K/2-1))}$ possible solutions. Initially, a population (i.e., set of solutions) is generated using the appropriate individuals (i.e., chromosomes that represent candidate optimum solution, $\alpha_{i,j}^{k}(t)$). This population is periodically updated using the crossover and mutation operations to generate individuals for the next generation. A typical chromosome structure is shown in Fig. 3.5. Then, the crossover operation is done in order to update the population by generating new offspring which enables to explore the search space for candidate solutions. After the crossover operation, the

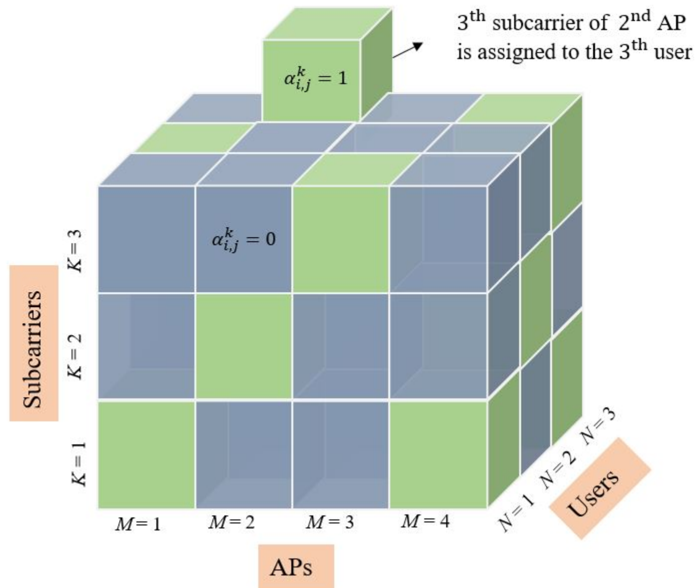

Figure 3.5: Chromosome structure (individual).

mutation operation is performed in order to increase the diversity of the population and avoid stopping at the local minimum values. Selection process is done to select the surviving individuals according to their fitness values. Candidate solutions among a huge solution set are intelligently explored and a set of chromosomes whose fitness values are higher are kept whereas others are eliminated in the selection phase. This process is repeated until the maximum number of iterations (i.e., stopping criterion) is reached. In our case, the fitness value of each individual is calculated according to the objective function in (3.28) and the maximum average optical power value, P_{av}, is used as a fixed power value of each APs. Intuitively, it is favorable to allocate more subcarriers to the set of users who have higher queue backlogs to achieve higher system throughput.

3.3.3 Power Control

Isolating $P_i(t)$ and removing other terms that do not contain $P_i(t)$, we can rewrite (3.25) as

$$\underset{P_i(t)}{\text{minimize}} \quad \sum_{i \in I} Y_i(t) P_i(t) - \sum_{j \in J} Q_j(t) \mu_j(t) \tag{3.29}$$

$$\text{subject to} \quad P_{\min} \leq P_i(t) \leq P_{\max}, \quad \forall i \in I. \tag{3.29a}$$

Using the fact that $\mu_j(t) \leq Z_j(t)$, the objective function (3.29) can be modified as follows

$$\underset{P_i(t)}{\text{minimize}} \quad \sum_{i \in I} Y_i(t) P_i(t) - \sum_{j \in J} Q_j(t) \left(\sum_{k=1}^{K} \sum_{i=1}^{M} \frac{\alpha_{i,j}^k(t)}{2\ln(2)} \frac{W}{K} \ln\left(1 + \frac{\exp(1)\gamma_{i,j}^k(t)}{2\pi}\right) T_s/S \right). \tag{3.30}$$

Due to the non-convexity of SINR, $\gamma_{i,j}^k(t)$, the solution of (3.30) is very difficult, if not impossible. Similar to previous sub-section, we resort to GA algorithm. The objective function in (3.30) is used to calculate the fitness values of each individual in GA-based power control algorithm. The individual with the best fitness value becomes the solution for the power control problem. The pseudo-code of the proposed resource management algorithm is given in Algorithm 3.1.

Algorithm 3.1 VLC Resource Management Algorithm.

while $t \leq T$ $(t \in [0, T])$ **do**
  for $j = 1$ to N **do**
    Obtain $f_j(t)$ according to (3.27);
    Obtain $\mu_j(t)$ and $a_{i,j}^k$ by GA;
    Update $Q_j(t+1)$ according to (3.6);
  end for
  for $i = 1$ to M **do**
    Obtain $P_i(t)$ by calling GA;
    Update $Y_i(t+1)$ according to (3.10);
  end for
end while

Table 3.1: Simulation parameters.

Parameters	**Values**
Size of room (L × W × H)	8 m × 8 m × 3 m
Number of luminary	4
Minimum power luminary	10 W
Maximum power luminary	60 W
View angle of luminary	40°
Distance between luminaries	3 m
Receiver FOV semi-angle	85°
Effective detection area	1 cm^2
Responsivity of PD	0.6 A/W
Vertical separation of transmitter and receiver	2.5 m
Noise density	1×10^{-20} A^2/Hz
AP signal bandwidth	20 MHz
DC bias factor	3
Number of subcarrier	16
Packet size	1000 bits
Time slot duration	1 ms

3.4 Numerical Results and Discussions

In the simulation setup we consider an empty room with a size of 8 m × 8 m × 3 m and there are 4 luminaries on the ceiling with equal distance each other. Each luminary has 40° half viewing angle. The height of the PD from the floor of the room is 0.5 m and effective detection area is 1 cm^2 area. PDs face upward towards the ceiling and FOV of them is 85°. The number of users varies from 10 to 24 and the number of subcarriers for each AP is 16. Users are initially assumed to be randomly located in the indoor environment and they change their location based on the RWP mobility model. The number of individuals in the initial population of GA is 8, and the number of GA iteration is set to 100. Each point of the simulations is averaged over 1000 time slots. Simulation parameters are summarized in Table 3.1.

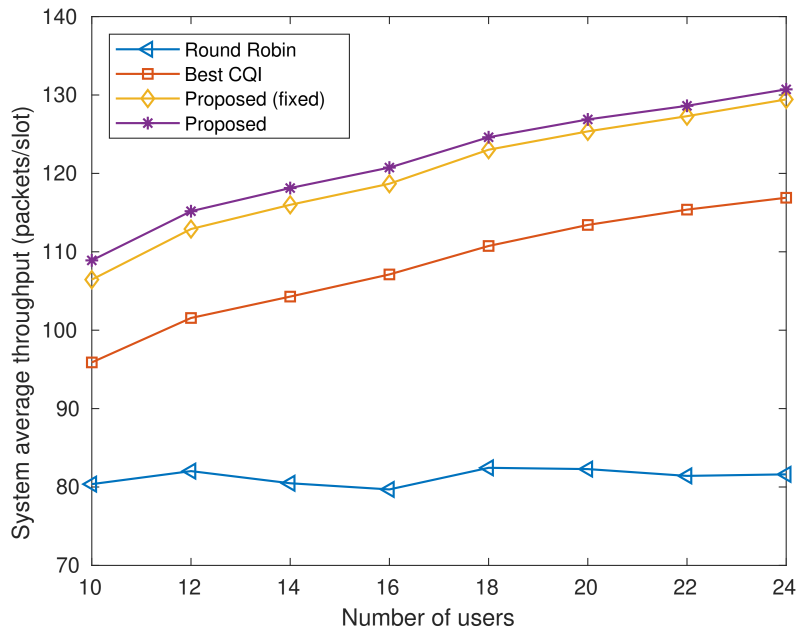

Figure 3.6: System average throughput versus number of users.

In Fig. 3.6 we present the average system throughput with respect to the number of users. As benchmarks, we consider two well-known resource allocation schemes, i.e., RR [109] and best CQI [110]. RR aims to equally allocate the resources among users to provide fairness. Best CQI algorithm is designed to give priority to the user with the best channel condition. We included two versions of proposed scheme with and without power control. It is observed that our proposed algorithm achieves higher average system throughput regardless of power control. Since the RR scheme does not consider channel state information and queue backlogs, it has the lowest system throughput. The Best CQI scheme outperforms the RR scheme because it takes into account the channel state information of each user.

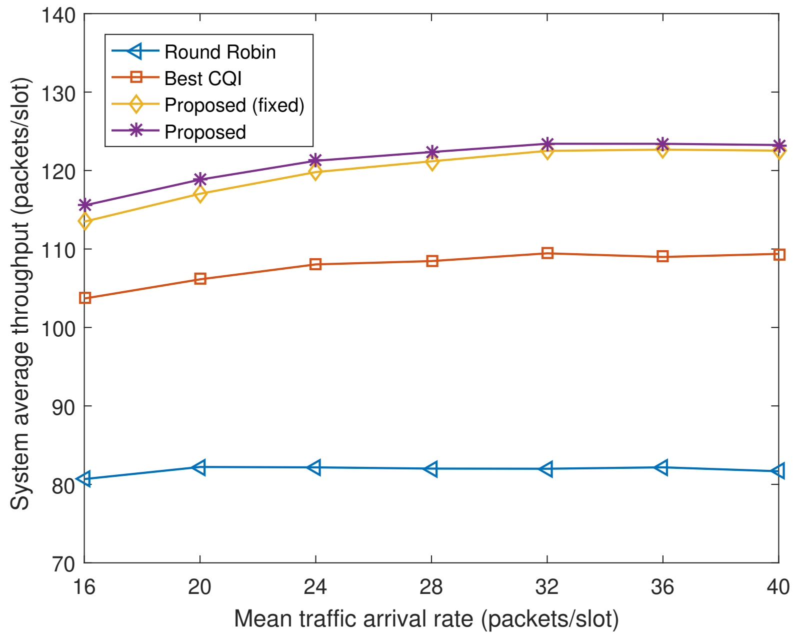

Figure 3.7: System average throughput versus mean traffic arrival rate.

Fig. 3.7 shows the average system throughput with respect to the different mean packet arrival rates. We assume that the number of users is 16, the maximum allowable average power of P_{av} is 30 W and V parameter is set as 300. It is observed that the average system throughput increases with respect to the mean packet arrival rates up to a certain value, this is because admission control mechanism rejects packets in order to ensure queue stability.

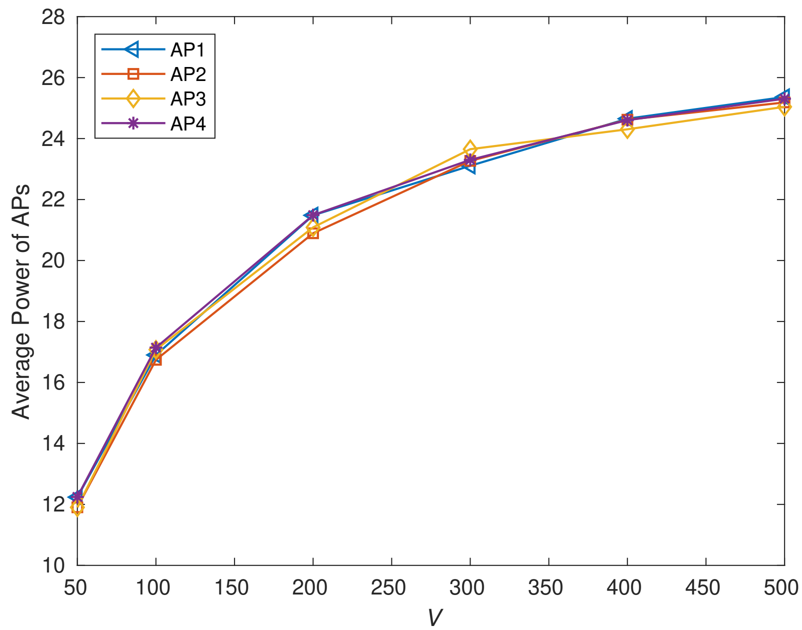

Figure 3.8: Average power of APs versus control parameter V.

Fig. 3.8 compares the average power consumption of APs for different values of V which is a tradeoff parameter between the system throughput and system constraints. In this simulation, we assume $N = 16$ users and average packet arrival rate of $\lambda_j = 24$ for each user. As seen in Fig. 3.8, the average power consumption increases with respect to V. A larger V enables the system to admit more packets into queues and delivering these packets require more power. In addition, it can be checked from Fig.3.8 that the average power consumption of APs satisfy the average power constraint.

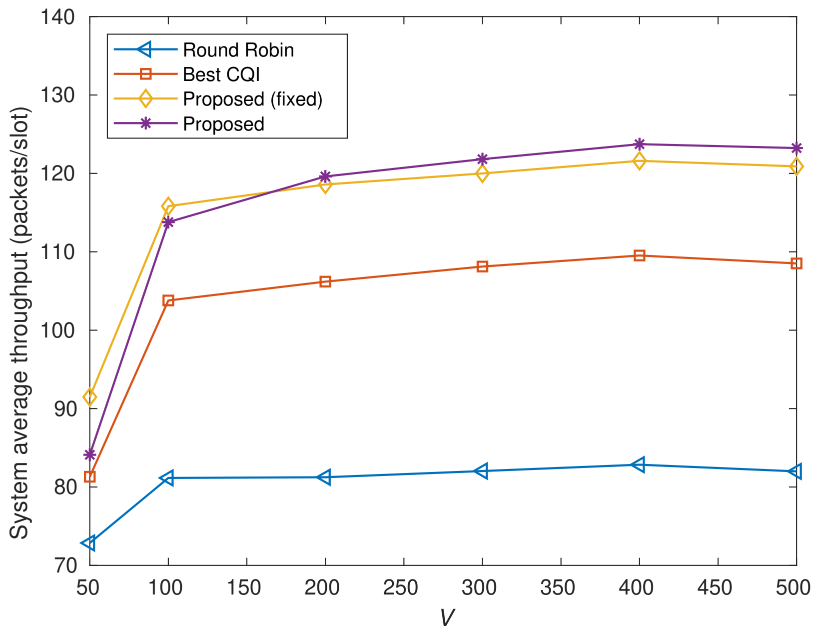

Figure 3.9: System average throughput versus control parameter V.

Fig. 3.9 shows the system throughput with respect to V. Since V is the control parameter used for tradeoff between the system constraints and the maximization of the system throughput, a larger V gives a higher priority on system throughput and enables the higher system performance.

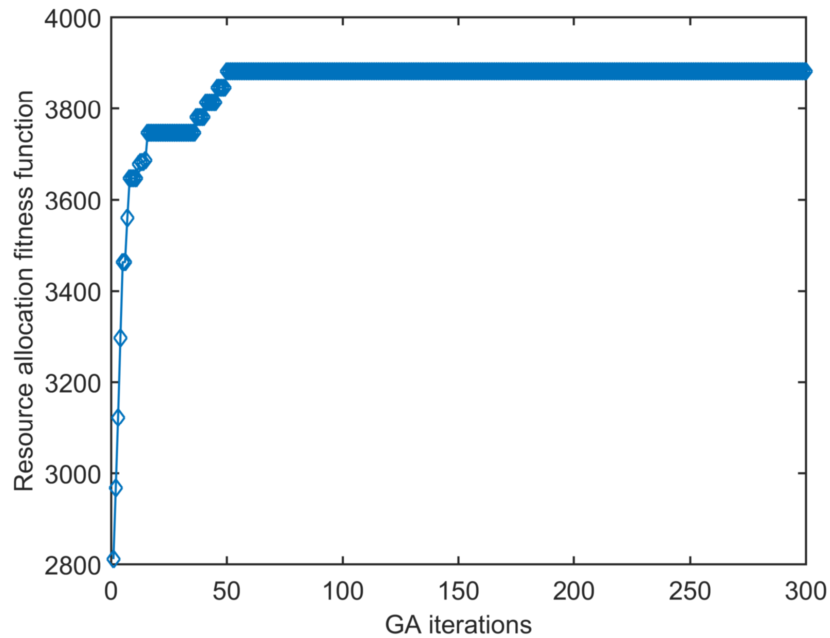

Figure 3.10: Convergence of GA resource allocation.

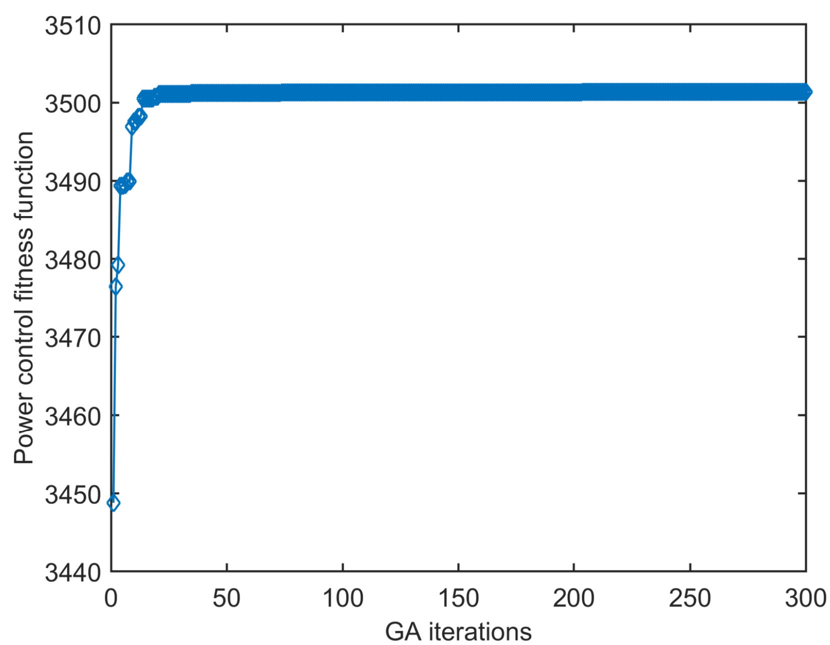

Figure 3.11: Convergence of GA power control.

In Fig. 3.10 and Fig. 3.11, we discuss the convergence properties of GA algorithm.

Fig. 3.10 shows the fitness function of the resource allocation problem with respect to the number of GA iterations. It is seen that GA based resource allocation algorithm converges around 60 iterations. Fig. 3.11 shows the fitness function of the power control problem, i.e., negative of equation (3.30), with respect to the number of GA iterations. It is observed that GA based power control algorithm converges after 40 iterations.

Table 3.2: Performance degradation due to the limited number of iterations.

Number of Iterations	**Average throughput (packets/slot)**	**Performance Degradation (%)**
60	121.8	0% (Reference value)
50	121.8	0%
40	118.6	2.6%
30	117.6	3.5%
20	117.6	3.5%
10	114.4	6.1%

As earlier emphasized, our proposed GA algorithm, if implemented on an FPGA platform, could be executed in a duration less than the time slot duration. However, it would be also interesting to quantify how much degradation in the performance should be expected if the execution time exceeds the time slot duration. In a case, where GA cannot reach the maximum iteration number due to a time constraint on execution time (for example, due to the limited capacity of computation platform, the execution time was restricted to remain less than the time slot duration), GA will return the current best solution as its outcome. In that case, termination criterion becomes the maximum time the algorithm will run. Table 3.2 lists the achieved average system throughputs for the number of iterations less than 60, i.e., convergence value (see

Fig. 3.10) and the corresponding degradations with respect to 121.8 packets/slot (which was achieved for 60 iterations). For example, assume that the GA algorithm is terminated after 30 iterations in order to remain within the execution time. In this case, the system throughput becomes 117.6 packets/slot, and this indicates only a 3.5% performance degradation.

CHAPTER IV

HANDOVER FOR INDOOR AND OUTDOOR VLC NETWORKS

This chapter focuses on mobility management techniques for indoor and outdoor VLC networks. In the first section, a CoMP joint-transmission based handover scheme is proposed for indoor VLC networks. In the second section, a dynamic velocity-aware handover algorithm is proposed for vehicular VLC networks.

4.1 Handover for Indoor VLC Networks with Coordinated Multipoint Transmission

In this section, we consider handover in an indoor VLC network with coordinated multipoint (CoMP) and evaluate its performance in physical channel settings based on ray tracing. In the VLC system under consideration, data to a single user is simultaneously transmitted from multiple APs to improve the received signal quality. Such joint transmission techniques, commonly referred to as CoMP, have been well investigated in the RF literature and already standardized in the LTE-A [111]. In the context of VLC, the only work that has earlier investigated CoMP is [112]; however handover is not addressed therein. In the VLC system under consideration, handover and CoMP decisions are carried out together based on the received signal strength of the mobile user. We compare the performance of proposed joint transmission-handover algorithm with hard handover and demonstrate significant performance gains in terms of user data rate. We also discuss the effect of channel models and show that the use of LOS model results in overestimation of the performance.

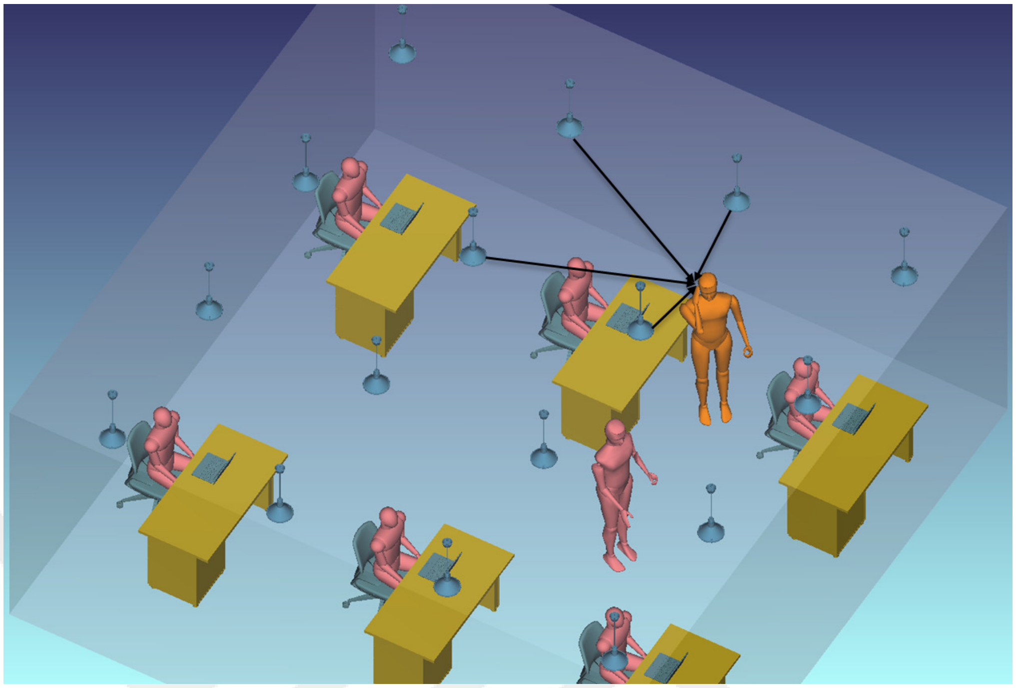

Figure 4.1: Office room under consideration.

4.1.1 System Model

As illustrated in Fig. 4.1, we consider a furnitured office room with a size of 7 m × 7 m × 3 m as an example for a realistic indoor environment. We assume 16 luminaries on the ceiling with equidistant spacing of 1.85 m in both x and y directions. These are commercially available LEDs (Cree® LR24-38SKA35) with 40° half viewing angle. The optical power for each luminary is 27 Watts. This yields an average illumination level of 526 lux which satisfies typical illumination levels for an office environment [113]. The uniformity, minimum and maximum illumination level are also 0.7, 365 lux, and 599 lux, respectively. The detector can be placed at any point, where the CIR is desired to be computed. Here, we assume that the user walks on a random trajectory (See Fig. 4.2) within the office room. We assume that he/she holds a cell phone in hand next to his/her ear and the detector is located on the phone. Specifically, we assume a detector height of 1.8 m with 45° rotation. The FOV and the area of the detector are 85° and 1 cm^2, respectively.

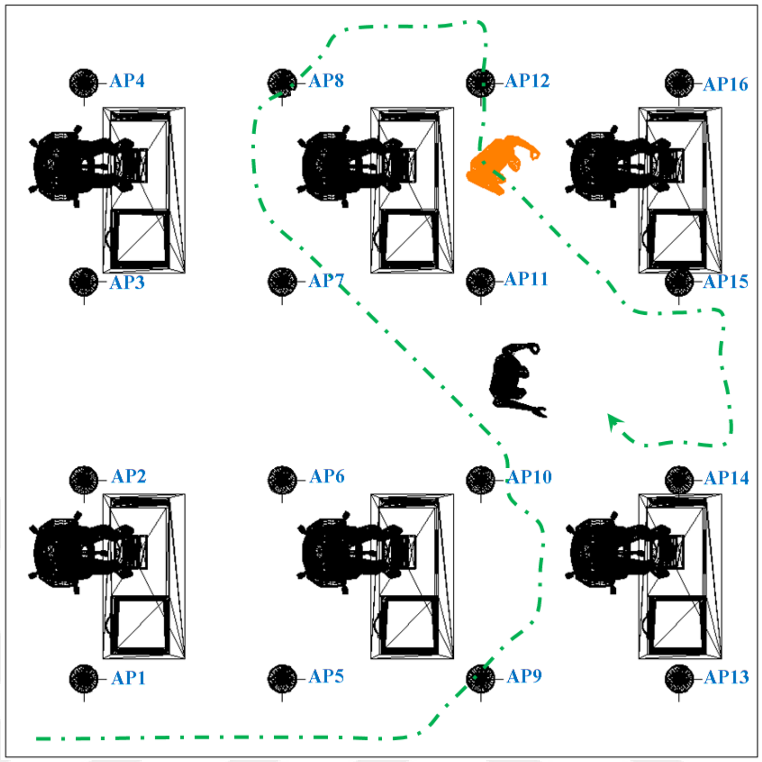

Figure 4.2: Movement trajectory of the user.

We consider an indoor VLC network with CoMP support. We assume the deployment of multiple ceiling luminaries each of which serves as an AP. Let AP_i denote the i^{th} AP, $i = 1, 2, ..., N_{\text{AP}}$. The user is mainly served by an AP (i.e., luminary) from which he/she gets the strongest signal. When the user moves towards the cell edge, the received signal from the served AP drops. Based on the handover algorithm decision, a handover to another AP can take place or CoMP is initiated. In the case of CoMP, the user is jointly served by two coordinating APs that transmit the same information.

The system model builds upon DCO-OFDM [19]. At the receiver, the time domain signal received by the user on subcarrier k can be expressed as

$$y_k(t) = R \sum\nolimits_{i \in S} H_i x_{i,k}(t) + R \sum\nolimits_{i \in U} H_i x_{i,k}(t) + n_k(t), \tag{4.1}$$

where S and U respectively denote the set of serving and interfering APs. Therefore, the first summation term represents the desired transmitted signals from APs serving the user and the second term denotes the received interference signal. In (4.1), $x_{i,k}(t)$ represents the corresponding transmitted signal component on subcarrier k and $n_k(t)$ denotes the noise signal with zero mean and variance of $\sigma_k^2 = N_0 W/K$, where N_0 is the noise PSD and W represents the modulation bandwidth.

As a performance metric to measure the quality of the communication link and transmission capacity, we adopt signal-to-interference-noise-ratio (SINR). Let η denote the DC-bias factor which determines the level of DC-bias depth [89]. SINR for subcarrier k can be expressed as

$$\gamma_k = \frac{R^2 \sum_{i \in S} H_i^2 E_{i,k}}{R^2 \sum_{i \in U} H_i^2 E_{i,k} + \sigma_k^2}, \tag{4.2}$$

where $E_{i,k}$ denotes the transmitted electrical signal power from AP_i on subcarrier k. Noting that only $K-2$ subcarriers carry data, where K represents the number of subcarriers. $E_{i,k}$ can be given by

$$E_{i,k} = \frac{\left(E\left[x_{i,k}(t)\right]\right)^2}{\eta^2\left(K-2\right)}. \tag{4.3}$$

Based on the Shannon channel capacity, the achievable data rate can be then calculated as

$$C = \sum_{k=1}^{K/2-1} (W/K)\log_2(1+\gamma_k). \tag{4.4}$$

4.1.2 Handover Technique

We assume that there is a centralized controller that is resposible for mobility management. The controller collects the users' received power information. Let $I_{R,i}$ denote the average received optical power (intensity) from AP_i. It can be calculated as [114] $I_{R,i} = H_i I_i,\ i = 1, 2, ..., N_{\text{AP}}$, where $I_i = E\left[x_i(t)\right] = x_{DC}$ is the average transmitted optical power. Furthermore, let $I_{R,C}$ and $I_{R,S}$ denote the received power from the candidate AP and the currently serving AP, respectively. The controller declares the AP with the highest received power as the candidate AP. If the serving AP has the stongest signal, the candidate AP will be the AP with the second highest received power.

In the joint transmission-handover algorithm under consideration, two conditions are checked to either make handover or start CoMP transmission. Similar to the well-known hard handover algorithm, a handover is triggered when the condition

$$I_{R,C} > I_{R,S} + HOM \tag{4.5}$$

is satisfied. Here, HOM stands for handover margin and represents the predefined hysteresis value which is used to avoid unnecessary handovers. When the user enters the region of candidate AP and the received power from that AP satisfies (4.5) for a certain time, then the user terminates its connection with source AP and connects to candidate AP. Therefore, candidate AP becomes the new source AP and starts serving the user alone.

In addition to (4.5), the following condition is checked:

$$I_{R,S} - HOM < I_{R,C} < I_{R,S} + HOM. \tag{4.6}$$

When the condition (4.5) is fulfilled, CoMP joint transmission starts and the user is jointly served by both APs. This condition shows that there is a candidate AP whose signal strength is not strong enough for handover decision but suitable for joint transmission. In CoMP phase, both APs transmit the same information and the received signals are combined in the receiver. If neither (4.5) nor (4.6) are satisfied, source AP will continue serving the user alone.

4.1.3 Simulation Results and Discussions

As discussed in Section 4.1.1, we consider a furnitured office room with 16 luminaries (APs) on the ceiling. The user walks on the specified trajectory (See Fig. 4.2) within the room. The main system parameters are summarized in Table 4.1.

In Fig. 4.3 and Fig. 4.4, we present the connectivity of the user for conventional hard handover (hard-HO) scheme in both channel models. In Fig. 4.3 and Fig. 4.4,

Table 4.1: Simulation parameters for scenario under consideration.

Parameters	**Values**
Size of room (L × W × H)	7 m × 7 m × 3 m
Room	Wall: Plaster Floor: Pinewood Ceiling: Plaster
Furniture	Desk: Pinewood Chair: Pinewood Laptop: Black gloss
Human CAD models	Heads: Absorbing Clothes: Cotton Shoes: Black gloss
Number of luminary	16
Power of each luminary	27 W
View angle of luminary	40°
Distance between luminaries	1.85 m
FOV of PD	85°
Area of PD	1 cm^2
Responsivity of PD	0.6 A/W
Vertical separation of transmitter and receiver	1.3 m
Noise density	1×10^{-20} A^2/Hz
DC bias factor	3
Number of subcarrier	512
HOM	7 dB

green dots show the locations of the mobile user and blue lines show which AP the user is connected to. Under the LOS channel model, the user is always served by the closest AP. However, in the physical channel model, the user is not necessarily always served by the closest AP as seen in the locations shown in a rectangle.

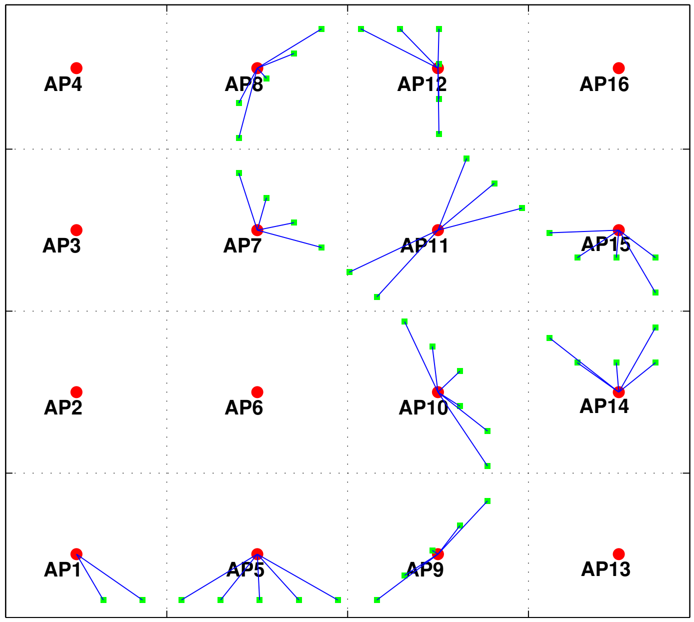

Figure 4.3: Connectivity graph of hard-handover algorithm for LOS channel.

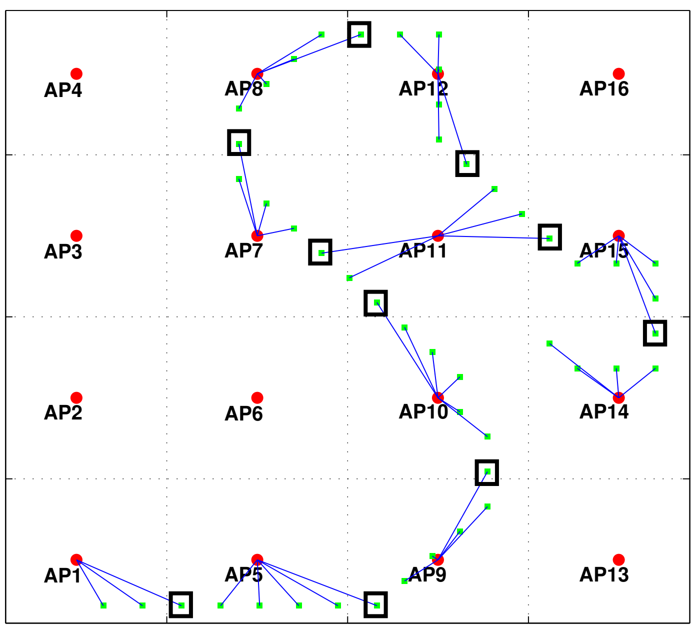

Figure 4.4: Connectivity graph of hard-handover algorithm for physical channel.

In Fig. 4.5, we present the Cumulative Distribution Function (CDF) of SINR for hard-HO scheme over LOS and physical channels. CDF of SINR graph gives the probability that SINR will take less than or equal to a specific value. It is observed that the system performance is overestimated in the LOS channel. There is about 9.3 dB median SINR difference between two channel models.

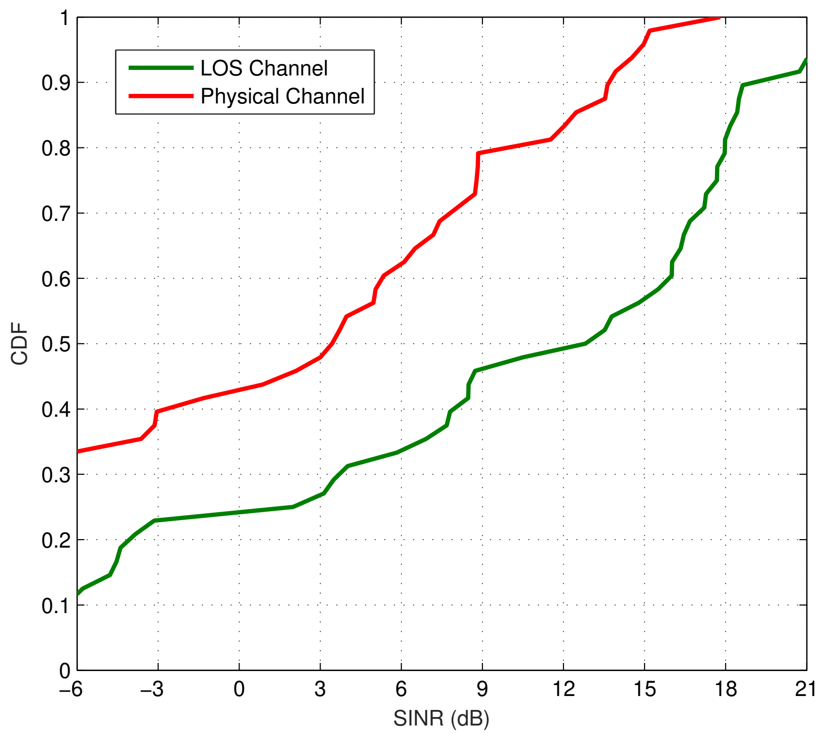

Figure 4.5: Performance of hard-handover over LOS and physical channels.

The performance difference between two models results from two reasons. First, the LOS channel model simply assumes that there is only direct received component ignoring the reflections from the walls and objects within the environment. Second, the rotation for the detector is precisely taken into account as the user moves in the physical channel in contrary to the LOS channel model [62, 63], where the receiver is always faced upwards to the ceiling with an elevation of 90°. Note that, LOS channel model in (1.1) takes into account rotation angle. However, this model is basically used for static scenarios and there is not an easy way to determine the rotation angle

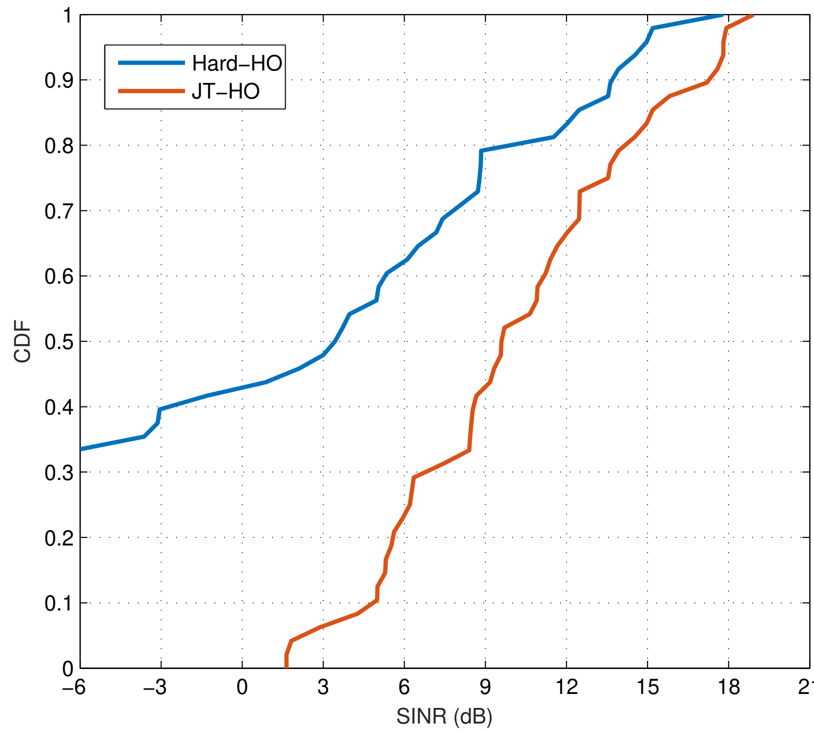

Figure 4.6: Comparison of hard-HO and JT-HO considering physical channel model.

for a moving user at each step. Therefore, similar to earlier works in [62, 63], we assume that the detector is placed upwards to the ceiling.

In Fig. 4.6, we present the performance comparison of hard-HO with our Joint Transmission-Handover (JT-HO) algorithm over the physical channel model. It is observed that the JT-HO algorithm outperforms the hard-HO scheme in terms of SINR. Specifically, JT-HO achieves a median SINR of 9.6 dB which is 6.2 dB better than the median SINR of the hard-HO.

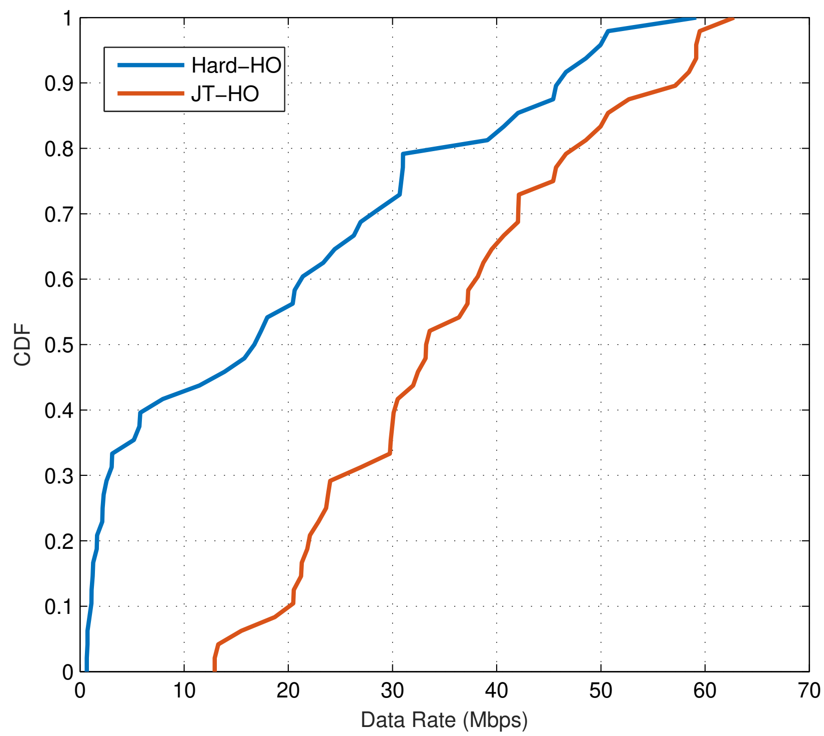

Figure 4.7: CDF of achievable data rate for hard-HO and JT-HO.

In Fig. 4.7, we present the CDFs of achievable data rate for hard-HO and JT-HO over physical channel model. It is observed from Fig. 4.7 that the advantage of using joint transmission is obvious in terms of the data rate. Since by using JT-HO algorithm, there will be a redundant connection, the optical VLC network is more robust to sudden connection drops.

4.2 CoMP-based Dynamic Handover for Vehicular VLC Networks

In this section, we propose a dynamic soft handover algorithm based on CoMP transmission. CoMP transmission has been well investigated in the wireless communication literature and already standardized in the LTE-A [111]. In the vehicular system under consideration, the centralized controller monitors the received power information reported from destination vehicle and decides which APs should serve the vehicle. The vehicle is mainly served by an AP from which it gets the strongest signal, but in the case of CoMP, the vehicle is jointly served by two coordinating APs. Based on the rate of change in the received powers (related to the vehicle velocity), the proposed handover algorithm dynamically revises the handover margin and time-to-trigger value in handover decision. In our algorithm, the handover margin typically increases while time-to-trigger value decreases for high-speed vehicles. This enables CoMP transmission to start early and maintain better signal quality. On the other hand, for low-speed vehicles, the handover margin is automatically set low and time-to-trigger value increases. This prevents the occurrence of ping-pong handovers and avoids unnecessary start of CoMP transmission in order to conserve the system resources. Ping-pong handovers occur when the user is handed over from one cell to another but is quickly handed back to the original cell. This causes unnecessary signaling overhead and is an indication of incorrect handover parameter settings. We evaluate the performance of proposed handover algorithm using realistic site-specific channel models developed through non-sequential ray tracing in OpticStudio® and demonstrate significant performance gains over conventional handover techniques.

4.2.1 System Model

As illustrated in Fig. 4.8, we consider a vehicular VLC network with multiple APs in the form of street light poles. The poles are uniformly arranged and separated from

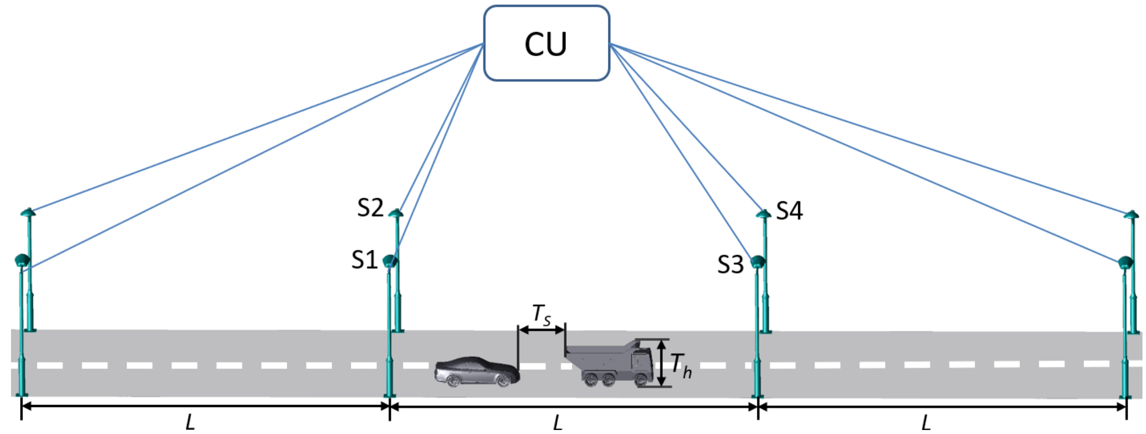

Figure 4.8: VLC-based I2V network.

each other with a spacing of L. The centralized CU and APs are connected with wired connections and the CU acts as a gateway to Internet. As illustrated in Fig. 4.9, we assume a two-lane highway road with a lane width of W_l. Each of light poles has a height of h, boom length (distance between the center of the pole and the luminaire) of B_l, and boom angle of θ. The street lights typically have an asymmetrical radiation pattern which features a narrow vertical beam angle combined with a wide horizontal beam one. The benefit of the horizontal wide beam angle is to spread the light to longer distances along the road while the vertical narrow beam is required in order to focus the light to the road surfaces only. We assume that the receiver (vehicle) is located at a distance of d_h (with respect to the road center) and travels with a velocity of v. It is equipped with a single photodetector located at the top of the car. It is possible that there might be other vehicles nearby, for example, a truck as illustrated in Fig. 4.8.

At the destination vehicle, the light intensity is detected by a photodetector. Let $H_i(t)$, $i = 1, ..., N_{AP}$, denote the DC channel gain from the i^{th} AP to the vehicle. The received signal can be given as [98]

$$y(t) = R\sqrt{P_e}\sum_{i\in \mathrm{S}} H_i(t)x_i(t) + R\sqrt{P_e}\sum_{j\in \mathrm{I}} H_j(t)x_j(t) + \upsilon(t), \tag{4.7}$$

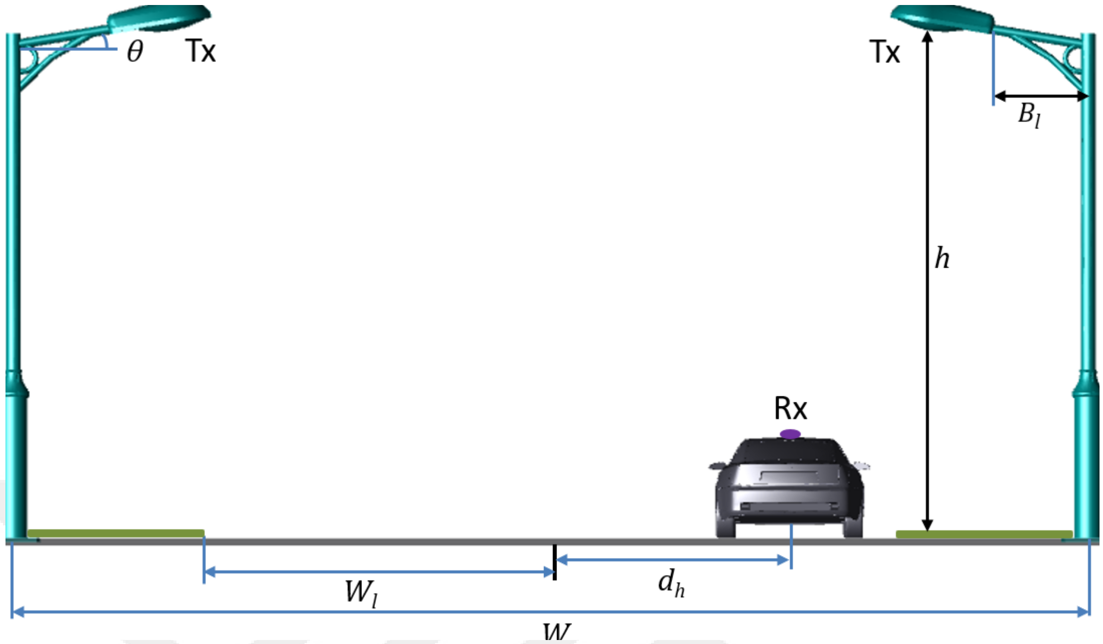

Figure 4.9: View from roadside.

where R represents the photodetector responsivity and P_e denotes the electrical power. It is possible to write the relationship between electrical power and optical power as $P_e = P_{\text{opt}}^2/\rho^2$ [98], where ρ is the electrical-to-optical conversion ratio. In the case of CoMP, the user is jointly served by coordinating APs that transmit the same information. Therefore, the set of S includes two APs, otherwise it is limited to a single serving AP. I denotes the set of interfering APs. In (4.7), $\upsilon(t)$ is the noise term with zero mean and variance of $\sigma^2 = N_0 B$. Here, N_0 is the noise PSD and B is the modulation bandwidth. Based on (4.7), the SINR at the destination vehicle can be expressed as [57]

$$\gamma(t) = \frac{\sum\limits_{i \in \mathrm{S}} P_i(t)}{\sum\limits_{j \in \mathrm{I}} P_j(t) + \sigma^2}, \tag{4.8}$$

where $P_i(t) = R^2 P_e H_i^2(t)$ is the received electrical power from the i^{th} AP.

4.2.2 CoMP based Dynamic Handover

Based on the received power strengths, the CU decides which APs should serve the vehicle. If there is a sufficiently strong AP signal, the vehicle is served by that specific AP. In transition regions between two cells, the vehicle is jointly served by two coordinating APs as a result of CoMP transmission. Based on the rate of change in the received powers, the proposed handover algorithm dynamically revises the Handover Margin (HOM) and Time-to-Trigger value (TTT) in handover decision.

Selection of HOM and TTT values are critical for vehicular networks. TTT value should be low for high-speed vehicles because when a rapidly moving vehicle approaches the cell edge, the received signal from the serving AP drops rapidly and handover should be triggered immediately. On the other hand, for low-speed vehicles, TTT value should be sufficiently high in order to prevent ping-pong effect. High-speed vehicles experience short dwell time that might cause connection losses due to the high handover rate. In order to improve the connectivity reliability, HOM value for high-speed vehicles should be set high compared to low-speed vehicles with relatively long cell dwell times. Unlike conventional CoMP, where fixed values of HOM and TTT are assumed, our proposed algorithm dynamically changes these threshold parameters.

The pseudo-code of the proposed handover algorithm is provided in Algorithm 4.1. Let $P_c(t)$ and $P_s(t)$ denote the received power from the candidate AP and the serving AP at time t, respectively. Furthermore, let $P_s(t-\Delta t)$ represent the received power from the serving AP at time $t-\Delta t$. The rate of the change in the received power is expressed as $\Delta P = [P_s(t) - P_s(t-\Delta t)]/\Delta t$. Based on the value of ΔP, HOM and TTT are respectively calculated as $HOM = \alpha\Delta P$ and $TTT = \lambda/\Delta P$, where α and λ are some constant coefficients. When a vehicle moves away from the serving AP, the received power of the serving AP decreases and the received power from the candidate AP increases. When the vehicle enters the region of the candidate AP and the condition $P_c(t) + HOM \geq P_s(t)$ is satisfied for a certain time, CoMP

Algorithm 4.1 Proposed Handover Algorithm.

```
for each $\Delta t$ do
    calculate rate of the change in received power
    $\Delta P = [P_s(t) - P_s(t - \Delta t)]/\Delta t$
    calculate $HOM = \alpha \Delta P$ and $TTT = \lambda / \Delta P$
    for each time slot do
        take measurements of $P_s(t)$ and $P_c(t)$
        if $P_c(t) \geq P_s(t) + HOM$ then
            if $handover\_timer \geq TTT$ then
                make handover
                reset $handover\_timer$, $CoMP\_timer$
            else
                if $CoMP\_timer \geq TTT$ then
                    start CoMP
                else
                    increment $handover\_timer$
                    increment $CoMP\_timer$
                end if
            end if
        else
            if $P_c(t) + HOM \geq P_s(t)$ then
                if $CoMP\_timer \geq TTT$ then
                    start CoMP
                else
                    increment $CoMP\_timer$
                end if
            end if
        end if
    end for
end for
```

transmission starts and the vehicle is jointly served by both serving and candidate APs. In CoMP phase, both APs transmit the same information and the received signals are combined at the receiver. Handover to the candidate AP is triggered when the $P_c(t) \geq P_s(t) + HOM$ is satisfied for a duration of TTT. The vehicle terminates its connection with the previous serving AP and continues getting service from the candidate AP. Therefore, candidate AP becomes the new serving AP and serves the vehicle alone until the new handover decision is taken.

A critical issue in the practical implementation is the choice of values of α and λ.

TTT is a monotonically increasing function of λ and a lower value of λ is preferred which expedites the start of handover and CoMP transmission, but the value of λ should be greater than 0 to prevent ping-pong handovers. On the other hand, HOM is a monotonically increasing function of α. The choice of too small α would disable the CoMP transmission while a large choice of α would trigger unnecessary CoMP transmissions. As a rule of thumb, α and λ values should be selected such that SINR remains almost constant regardless of the vehicle speed.

4.2.3 Simulation Results and Discussions

In our simulations, we consider a two-lane road, where the poles in the same lane are separated with a spacing of $L = 20$ m, and each of them has a height of $h = 7$ m. The boom length is assumed to be $B_l = 1$ m, and the boom angle is considered as $\theta = 10°$. The coating materials of road surface, cars, and streetlamp poles are assumed as asphalt, black gloss paint, and galvanized steel metal, respectively. We consider a commercial streetlamp with an asymmetrical radiation pattern [115]. We consider two main use cases: **Scenario A.** The car travels in the right lane without any neighbor vehicles, **Scenario B.** The car travels in the right lane and precedes a loaded truck with a height of $T_h = 4.2$ m. The distance between two vehicles is given by $T_s = 4$ m. The second scenario is particularly useful to analyze the effect of potential blockage. The dimensions of the car and the loaded truck are respectively 4.6 m × 1.8 m × 1.3 m and 5.4 m × 1.8 m × 4.2 m. The car is equipped with a single photodetector located at the top of the car (See Fig. 4.9). It has an aperture area of 10 mm × 15 mm and FOV angle of 180°. A lower value of FOV will reduce the ambient noise. However, in an interference-limited case, this reduction will be negligible. Therefore, we preferred a wide FOV angle to maximize the reception angle in mobile conditions under consideration. All simulation parameters are summarized in Table 4.2. The three dimensional simulation environment is constructed in OpticStudio®

software. CIRs between each street light and destination vehicle are obtained based on non-sequential ray tracing features of this software (see [116] for details on channel modeling) at each 1 meter over the traveling distance between two poles. Based on earlier discussions in Section 4.2.2, constant coefficients α and λ are set as 200 and 0.1, respectively.

Table 4.2: Simulation parameters for vehicular handover.

Parameters	**Values**
Road specifications	Type: R2 Material: Asphalt Lane width: 3.75 m Road width: 10.5 m Number of lanes: 2
Vehicle specifications	Length: 4.673 m Width: 1.846 m Height: 1.371 m Material: Black paint
Poles specifications	Arrangement: Opposing Material: Galvanized steel Spacing: 20 m Height: 7 m Boom Length: 1 m Boom Angle: 10°
Transmitter specifications	Type: Street lamp Brand: Ephesus M3S 90 Optical power: 1 W Power ratio: 3
FOV of PD	180°
Area of PD	150 mm^2
Responsivity of PD	1 A/W
Noise density	1×10^{-20} A^2/Hz
Bandwidth	20 MHz

In Fig. 4.10, we consider Scenario A (i.e., without blockage case) and assume that the car travels in the middle of the right lane (i.e., $d_h = 2$ m). We present the average HOM and TTT values as a function of the vehicle speed to better highlight the necessity of dynamically revising these parameters which is the main feature of

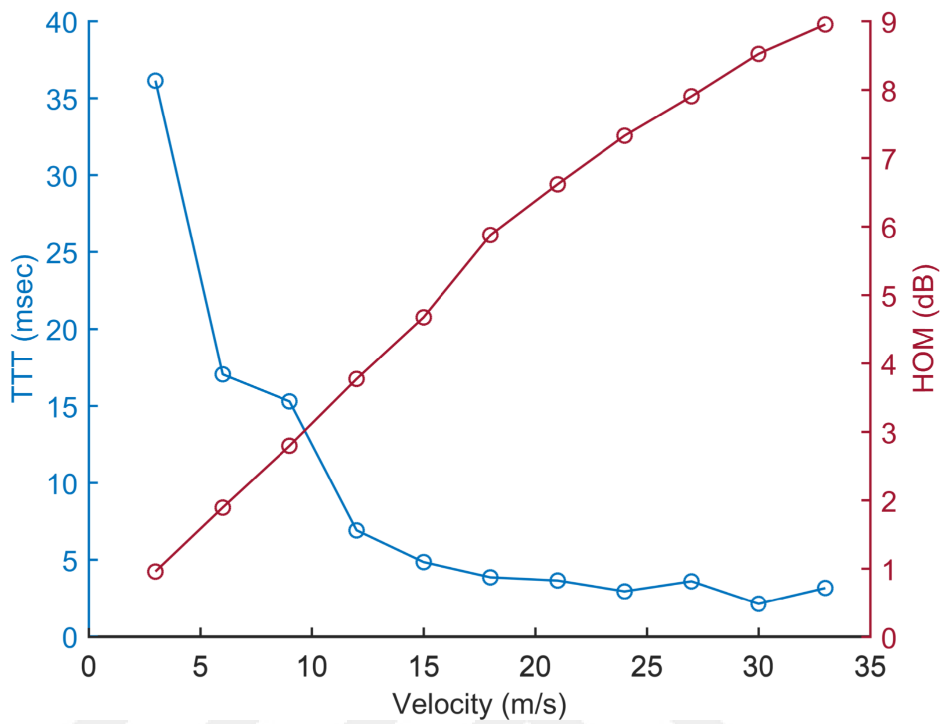

Figure 4.10: *HOM* and *TTT* versus velocity.

the proposed algorithm. It is observed that *TTT* decreases with velocity. Since, the received signal drops rapidly for high-speed vehicles when they move away from the source, AP handover is initiated more rapidly for them in comparison to slower vehicles. On the other hand, *HOM* increases with speed. For high-speed vehicles, CoMP transmission starts earlier and continues longer. This makes system more reliable to sudden connection drops due to high velocity. Consequently, there is a combination of proper *HOM* and *TTT* values that needs to be selected for each speed of the vehicle.

In Fig. 4.11, we present the performance of proposed handover algorithm for Scenario A. We assume that the vehicle travels at the center of lane with the speed of 18 m/s (= 64.8 km/hr). As benchmarks, we consider four schemes: **1.** Hard handover as specified in 3GPP document [117], **2.** Best Connection (BC) algorithm [118], where the vehicle is always connected to the AP providing the received signal with the highest power, **3.** Conventional CoMP handover, where the user can be jointly served

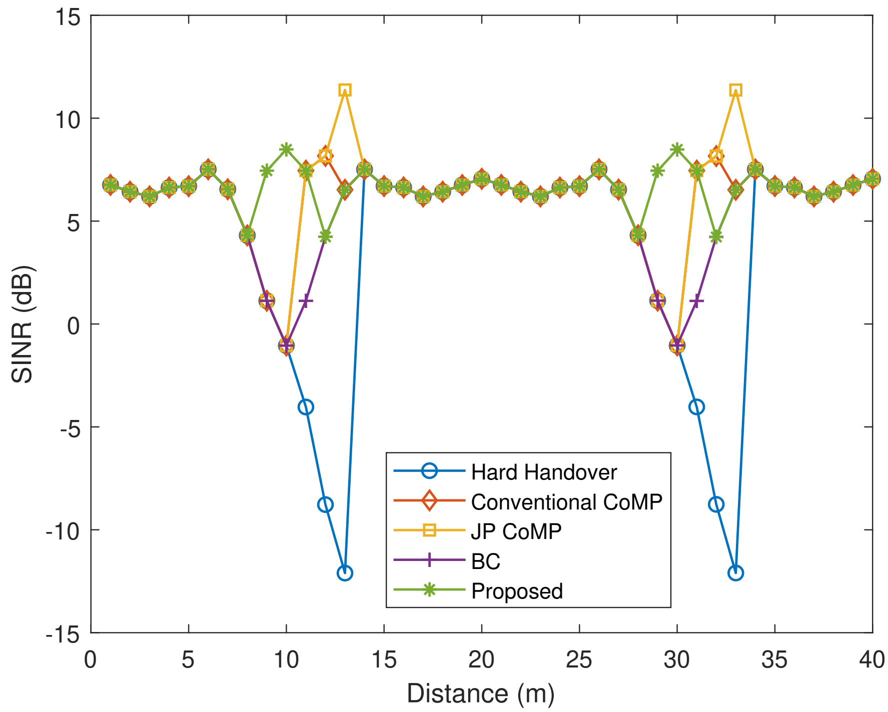

Figure 4.11: Performance comparison of proposed handover algorithm.

by two coordinating APs, **4.** CoMP-Joint Processing (CoMP-JP) handover [119] which uses the average power of the received signals from the coordinated APs instead of the power of the received signal from the source AP (allowing the postponement of the handover if necessary).

In hard handover, handover margin is set as $HOM = 1$ dB while time-to-trigger is set as $TTT = 160$ ms in order to prevent ping-pong handovers [75]. In conventional CoMP, fixed parameters of $HOM = 3$ dB value and $TTT = 80$ ms value are assumed. Fixed values of HOM and TTT are used in conventional CoMP algorithm. Therefore, it is important to choose values which will provide a decent performance independent of the vehicle speed. In order to determine proper values, we simulated the performance of conventional CoMP for different HOM and TTT values assuming vehicle speeds of 9 m/s, 18 m/s and 27 m/s. Based on these extensive simulations, we selected $HOM = 3$ dB and $TTT = 80$ ms which maintain a relatively stable SINR and fit better for all speeds. The same values are also employed in CoMP-JP. It is reported in [119] that CoMP-JP provides a superior performance for 2 dB $< HOM <$ 4 dB. In BC algorithm, in order to connect to the AP providing the received signal with highest power, $HOM = 0$ dB and $TTT = 0$ ms are chosen as default. In the proposed algorithm, it can be readily checked from Fig. 4.10 that HOM and TTT values should be chosen respectively as $HOM = 5.90$ dB and $TTT = 3.85$ ms for the speed of 18 m/s under consideration.

It is observed from Fig. 4.11 that hard handover, conventional CoMP, CoMP-JP, and BC algorithms have severe fluctuations in SINR. In hard handover, SINR drops as low as -12.1 dB while lowest values experienced in conventional CoMP, CoMP-JP and BC handover schemes are significantly larger. CoMP-JP algorithm has similar performance to conventional CoMP, but at cell edges it triggers unnecessary CoMP transmission and causes unnecessary usage of system resources. On the other hand, as a result of the proper selection of HOM and TTT values, the proposed handover technique maintains a more stable SINR and outperforms its counterparts. The lowest SINR value is obtained as 4.23 dB which is much higher than those in benchmarking schemes and therefore enables a better signal quality.

In Fig. 4.12, we investigate the effect of vehicle speed on the performance of proposed handover algorithm assuming Scenario A. We consider three different speeds: 9 m/s (= 32.4 km/hr), 18 m/s (= 64.8 km/hr) and 27 m/s (= 97.2 km/hr). It is assumed that the vehicle travels at the center of lane. HOM and TTT values are selected as $\{HOM = 2.80, TTT = 15.28\}$ for 9 m/s, $\{HOM = 5.90, TTT = 3.85\}$ for 18 m/s, $\{HOM = 7.89, TTT = 3.60\}$ for 27 m/s. It is observed that the proposed algorithm is able to maintain a stable SINR performance regardless of the vehicle speed. The average SINR values for 9 m/s, 18 m/s and 27 m/s can be calculated respectively as 6.63 dB, 6.63 dB and 6.99 dB. Similarly, the lowest SINR value experienced for different speeds remains around 4.25 dB. These results demonstrate the performance stability of proposed algorithm for different speeds.

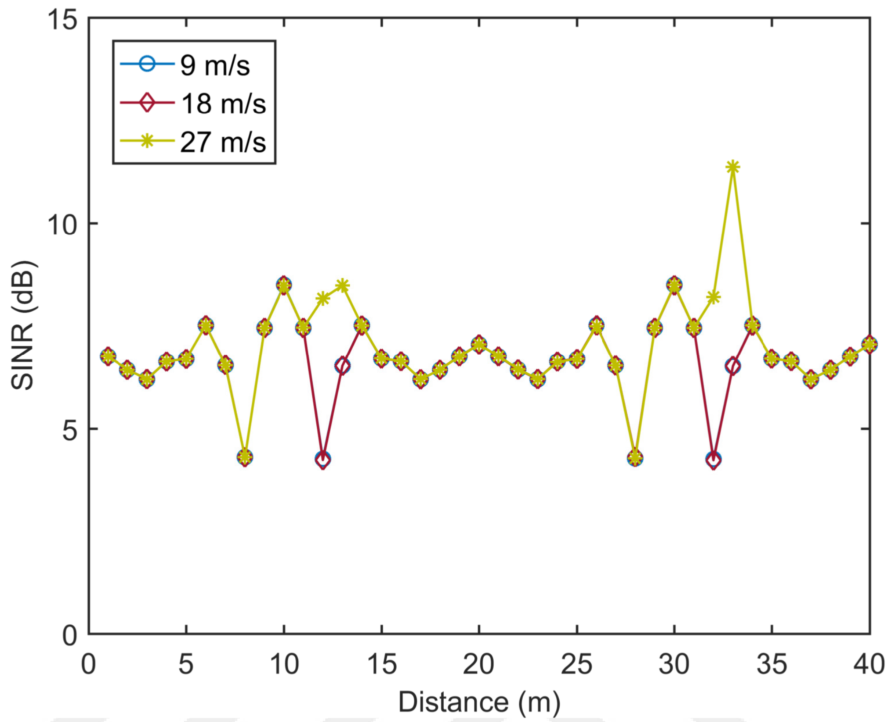

Figure 4.12: SINR versus distance with different vehicle speeds.

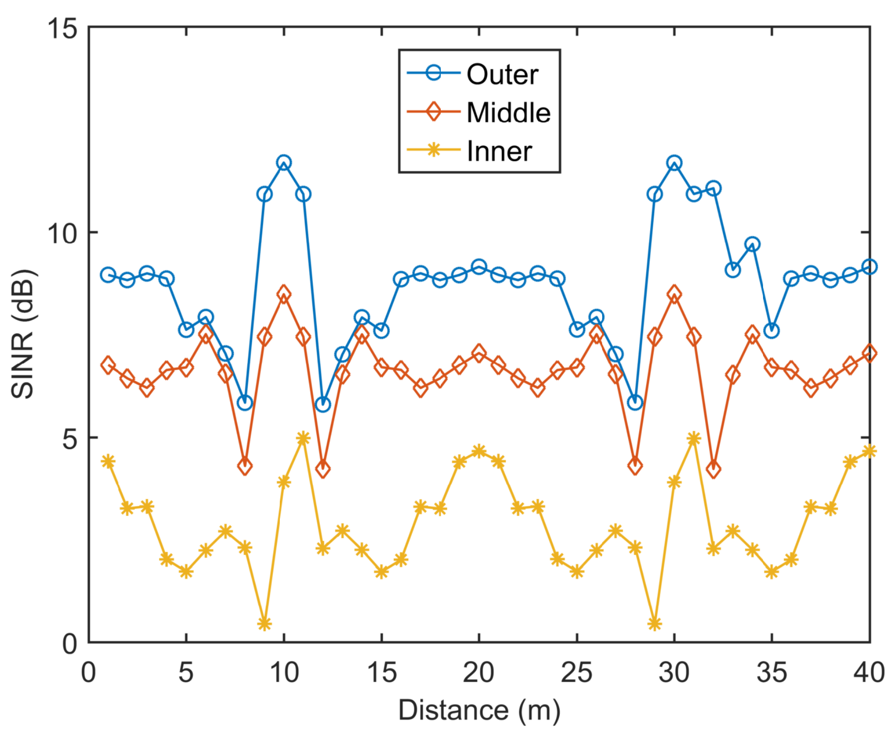

Figure 4.13: SINR versus distance for proposed handover technique.

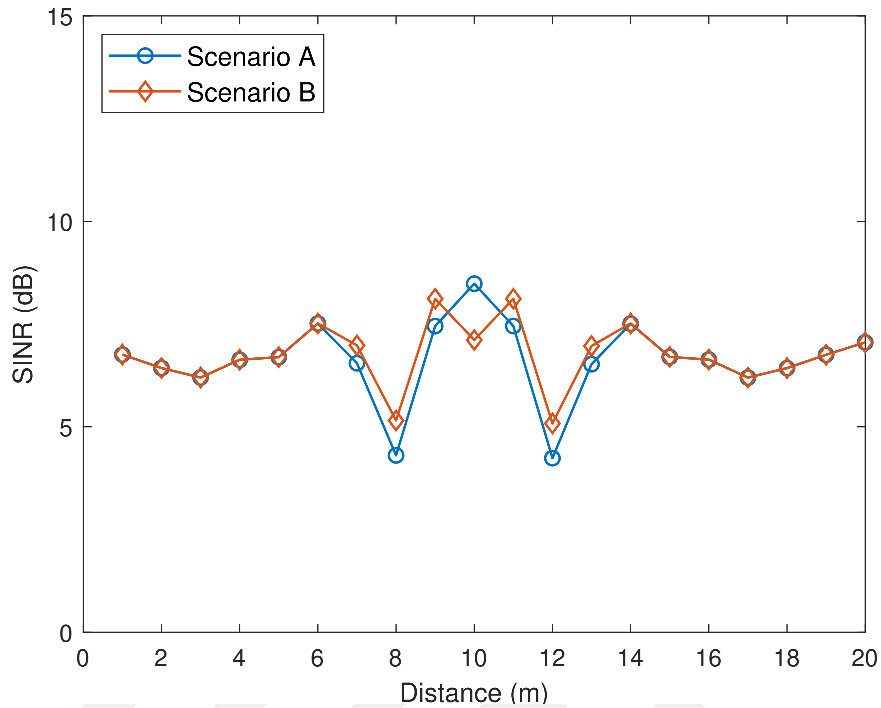

Figure 4.14: Effect of blockage on the performance of proposed handover algorithm.

In Fig. 4.13, we present SINR of proposed algorithm for different locations of the vehicle within the right lane. We assume three distinct locations for the vehicle, specifically the vehicle travels a) in the inner side of the right lane, i.e., d_h =1 m, b) in the outer side of the right lane, i.e., d_h =3 m, or c) at the middle of the right lane, i.e., d_h = 2 m. It is assumed that the speed of car is 18 m/s (= 64.8 km/hr). When vehicle travels in the outer side of the lane, it gets closer to the right side poles and away from the interfering poles on the other side; therefore, it has better SINR performance compared to other locations. For example, on the average, the vehicle in the outer side (i.e.,d_h =3 m) experiences 3.18 dB higher SINR than the vehicle in the middle of lane. On the other hand, the SINR value for the vehicle in the inner side (i.e.,d_h =1 m) drops about 5.88 dB on the average.

In Fig. 4.14, we investigate the effect of blockage on the proposed handover algorithm. The blue plot is obtained for Scenario A (i.e., without blockage) while the orange plot is obtained for Scenario B (i.e., with blockage). It is observed that blockage introduces some degradation around $d = 10$ m which corresponds to midway between two APs. Because at the cell edge, the vehicle is jointly served by S1 and S3 and, since the received power from S3 in Scenario B is lower than that received in Scenario A due to blockage, some degradation in SINR value is observed. Other than the cell edge, SINR values for blockage and non-blockage scenarios remain nearly the same in general. Interestingly, between 6 m $< d <$ 10 m and 10 m $< d <$ 14 m, SINR values in blockage case are even slightly higher than those in non-blockage case. For 6 m $< d <$ 10 m, the car is served by S1 located behind the truck and the blockage reduces the interfering signal that comes from S3. Therefore, the blockage becomes beneficial in this case since it partially obstructs the interfering signal. Similarly, for 10 m $< d <$ 14 m, the car is served by S3 while the received power from S4 (interfering signal) is reduced due to the blockage effect.

CHAPTER V

CONCLUSIONS

There has been an increasing attention on visible light communications in the last few years. Current studies of point-to-point VLC systems in the literature are well established and especially the studies on physical layer aspects show the potential of VLC. However, significant further efforts on upper layer issues are necessary to transform VLC to a multiuser, multicell, scalable, and fully networked wireless access technology. In this dissertation, we investigate resource allocation and mobility management techniques for indoor and vehicular VLC systems.

In Chapter II, we have considered a centralized DCO-OFDM based VLC network, where multiple LEDs serve as APs for a number of mobile users. Taking into account that users have data rate requirements, we have formulated a subcarrier resource allocation problem to maximize the user satisfaction index. For the solution of resulting constrained nonlinear integer programming problem, we used bio-inspired PSO method. In each time interval, based on the channel state information and the data rate requirements of the users as well as the overload status of the APs, the proposed algorithm decides which AP will serve a specific user and which subcarriers of that AP will be assigned to that user. If there are overloaded APs, the algorithm handovers the users to the neighbor available APs. If the mobile user experiences unfavorable channel conditions due to its location, the algorithm handovers the user to another available AP with better channel conditions. We have conducted a simulation study to investigate the system throughput and satisfaction index. Our numerical results have clearly demonstrated the superiority of the proposed algorithm over Round Robin, Best CQI and Genetic algorithms.

In Chapter III, we propose an energy efficient dynamic resource management mechanism for indoor OFDM-based VLC networks. Specifically, we formulate and investigate a stochastic cross-layer optimization problem to optimize the network resources under the constraints of queue stability and power to maximize the average system throughput. By using the Lyapunov optimization technique, we convert the long term time-average optimization problem into a series of single time slot online problems. Then, we decompose the problem into independent deterministic packet admission, resource allocation and power control sub-problems. We propose a simple threshold based admission control algorithm and GA-based resource allocation and power control algorithm to maximize the system throughput. Simulation results show that our technique provides an improved system performance while satisfying the system constraints.

In Chapter IV, we investigate handover algorithms for indoor and outdoor VLC networks. First, we have proposed a handover scheme combined with joint transmission for VLC networks. We have used a physical channel model based on ray tracing which allows an accurate description of the interaction of rays emitted from the lighting source within a specified indoor environment. Our results have demonstrated that the conventional LOS channel model overestimates the performance and might be misleading. Under the adopted physical channel model, we have shown that joint transmission-handover algorithm provides significant performance gains over hard handover schemes.

Then, we have proposed a velocity-aware coordinated multipoint (CoMP) transmission based dynamic handover algorithm for vehicular VLC networks. The vehicle is mainly served by an access point (AP) from which it gets the strongest signal. When the vehicle moves towards the cell edge, CoMP transmission is initiated and the user is jointly served by coordinating APs that transmit the same information.

Unlike the conventional CoMP, the proposed algorithm dynamically revises the handover margin (HOM) and time-to-trigger (TTT) values based on the rate of change in the received power. Our simulation results show that TTT should take small values for high-speed vehicles while it increases for low-speed vehicles in order to prevent ping-pong effect. On the contrary, HOM should take high values for high-speed vehicles while it should decrease for low-speed vehicles with relatively long cell dwell times. With proper selection of HOM and TTT values, our proposed algorithm outperforms the conventional CoMP and hard handover and maintains higher and more stable SINR performance. Our simulation results further reveal that the proposed algorithm provides a stable performance even in the presence of nearby vehicles which can result in partial blockage of the received signal.

Bibliography

[1] O. Narmanlioglu, *Visible light communications with advanced physical layer features and integration with existing wireless communication technologies*. PhD thesis, Özyeğin University, 2020.

[2] Z. Ghassemlooy, S. Arnon, M. Uysal, Z. Xu, and J. Cheng, "Emerging optical wireless communications-advances and challenges," *IEEE Journal on Selected Areas in Communications*, vol. 33, no. 9, pp. 1738–1749, 2015.

[3] T. Komine and M. Nakagawa, "Fundamental analysis for visible-light communication system using LED lights," *IEEE Transactions on Consumer Electronics*, vol. 50, no. 1, pp. 100–107, 2004.

[4] E. Basar, M. Wen, R. Mesleh, M. Di Renzo, Y. Xiao, and H. Haas, "Index modulation techniques for next-generation wireless networks," *IEEE Access*, vol. 5, pp. 16693–16746, 2017.

[5] L. U. Khan, "Visible light communication: applications, architecture, standardization and research challenges," *Digital Communications and Networks*, vol. 3, no. 2, pp. 78–88, 2017.

[6] L. Grobe, A. Paraskevopoulos, J. Hilt, D. Schulz, F. Lassak, F. Hartlieb, C. Kottke, V. Jungnickel, and K.-D. Langer, "High-speed visible light communication systems," *IEEE Communications Magazine*, vol. 51, no. 12, pp. 60–66, 2013.

[7] F. Miramirkhani and M. Uysal, "Channel modeling and characterization for visible light communications," *IEEE Photonics Journal*, vol. 7, no. 6, pp. 1–16, 2015.

[8] Z. Chen, *Interference mitigation techniques for optical attocell networks.* PhD thesis, The University of Edinburgh, 2017.

[9] S. Dimitrov and H. Haas, *Principles of LED light communications: towards networked Li-Fi.* Cambridge University Press, 2015.

[10] P. H. Pathak, X. Feng, P. Hu, and P. Mohapatra, "Visible light communication, networking, and sensing: a survey, potential and challenges," *IEEE Communications Surveys & Tutorials*, vol. 17, no. 4, pp. 2047–2077, 2015.

[11] D.-s. Shiu and J. M. Kahn, "Differential pulse-position modulation for power-efficient optical communication," *IEEE Transactions on Communications*, vol. 47, no. 8, pp. 1201–1210, 1999.

[12] B. Bai, Z. Xu, and Y. Fan, "Joint LED dimming and high capacity visible light communication by overlapping PPM," in *Proc. IEEE Annual Wireless and Optical Communications Conference (WOCC)*, pp. 1–5, 2010.

[13] H. Sugiyama and K. Nosu, "MPPM: A method for improving the band-utilization efficiency in optical PPM," *Journal of Lightwave Technology*, vol. 7, no. 3, pp. 465–472, 1989.

[14] M. A. Khalighi and M. Uysal, "Survey on free space optical communication: a communication theory perspective," *IEEE Communications Surveys & Tutorials*, vol. 16, no. 4, pp. 2231–2258, 2014.

[15] *Standard for Local and Metropolitan Area Networks-Part 15.7: Short-Range Wireless Optical Communication Using Visible Light.* IEEE 802.15.7, 2011.

[16] S. Idris, A. M. Aibinu, G. Koyunlu, and J. Sanusi, "A survey of modulation schemes in visible light communications," in *Proc. IEEE International Conference on Trends in Electronics and Informatics (ICOEI)*, pp. 1–7, 2019.

[17] M. A. Kashani and M. Kavehrad, "On the performance of single-and multi-carrie modulation schemes for indoor visible light communication systems," in *Proc. IEEE Global Communications Conference (GLOBECOM)*, pp. 2084–2089, 2014.

[18] L. Wu, Z. Zhang, J. Dang, and H. Liu, "Adaptive modulation schemes for visible light communications," *Journal of Lightwave Technology*, vol. 33, no. 1, pp. 117–125, 2014.

[19] J. Armstrong, "OFDM for optical communications," *Journal of Lightwave Technology*, vol. 27, no. 3, pp. 189–204, 2009.

[20] Q. Li, T. Baykas, and V. Jungnickel, "IEEE 802.15.13 multi giga bit/sec optical wireless communication project," *IEEE COMSOC MMTC Communications*, vol. 13, pp. 34–38, 2018.

[21] *Standard for Information Technology-Telecommunications and Information Exchange Between Systems Local and Metropolitan Area Networks-Specific Requirements, Part 11: Wireless LAN Medium Access Control (MAC) and Physical Layer(PHY) Specifications Amendment: Light Communications.* IEEE 802.11bb, 2018.

[22] E. Lam, S. K. Wilson, H. Elgala, and T. D. Little, "Spectrally and energy efficient OFDM (SEE-OFDM) for intensity modulated optical wireless systems," *arXiv preprint arXiv:1510.08172*, 2015.

[23] H. A. Omar, K. Abboud, N. Cheng, K. R. Malekshan, A. T. Gamage, and W. Zhuang, "A survey on high efficiency wireless local area networks: Next generation WiFi," *IEEE Communications Surveys & Tutorials*, vol. 18, no. 4, pp. 2315–2344, 2016.

[24] J. G. Andrews, T. Bai, M. N. Kulkarni, A. Alkhateeb, A. K. Gupta, and R. W. Heath, "Modeling and analyzing millimeter wave cellular systems," *IEEE Transactions on Communications*, vol. 65, no. 1, pp. 403–430, 2016.

[25] Z. Ghassemlooy, L. N. Alves, S. Zvanovec, and M.-A. Khalighi, *Visible light communications: theory and applications*. CRC press, 2017.

[26] L. E. M. Matheus, A. B. Vieira, L. F. Vieira, M. A. Vieira, and O. Gnawali, "Visible light communication: concepts, applications and challenges," *IEEE Communications Surveys & Tutorials*, vol. 21, no. 4, pp. 3204–3237, 2019.

[27] S. Kumar and P. Singh, "A comprehensive survey of visible light communication: potential and challenges," *Wireless Personal Communications*, vol. 109, no. 2, pp. 1357–1375, 2019.

[28] H. Haas, L. Yin, Y. Wang, and C. Chen, "What is LiFi?," *Journal of Lightwave Technology*, vol. 34, no. 6, pp. 1533–1544, 2016.

[29] R. Bai, H. Tian, B. Fan, and S. Liang, "Coordinated transmission based interference mitigation in VLC network," in *Proc. IEEE Vehicular Technology Conference (VTC)*, pp. 1–5, 2015.

[30] X. Li, F. Jin, R. Zhang, J. Wang, Z. Xu, and L. Hanzo, "Users first: user-centric cluster formation for interference-mitigation in visible-light networks," *IEEE Transactions on Wireless Communications*, vol. 15, no. 1, pp. 39–53, 2016.

[31] S. Shao, A. Khreishah, and I. Khalil, "Joint link scheduling and brightness control for greening VLC-based indoor access networks," *Journal of Optical Communications and Networking*, vol. 8, no. 3, pp. 148–161, 2016.

[32] M. Obeed, A. M. Salhab, M.-S. Alouini, and S. A. Zummo, "On optimizing VLC networks for downlink multi-user transmission: a survey," *IEEE Communications Surveys & Tutorials*, vol. 21, no. 3, pp. 2947–2976, 2019.

[33] S. Al-Ahmadi, O. Maraqa, M. Uysal, and S. M. Sait, "Multi-user visible light communications: state-of-the-art and future directions," *IEEE Access*, vol. 6, pp. 70555–70571, 2018.

[34] Y. Tao, X. Liang, J. Wang, and C. Zhao, "Scheduling for indoor visible light communication based on graph theory," *Optics Express*, vol. 23, no. 3, pp. 2737–2752, 2015.

[35] F. Jin, X. Li, R. Zhang, C. Dong, and L. Hanzo, "Resource allocation under delay-guarantee constraints for visible-light communication," *IEEE Access*, vol. 4, pp. 7301–7312, 2016.

[36] R. K. Mondal, M. Z. Chowdhury, N. Saha, and Y. M. Jang, "Interference-aware optical resource allocation in visible light communication," in *Proc. IEEE International Conference on ICT Convergence (ICTC)*, pp. 155–158, 2012.

[37] O. Babatundi, L. Qian, and J. Cheng, "Downlink scheduling in visible light communications," in *Proc. IEEE International Conference on Wireless Communications and Signal Processing (WCSP)*, pp. 1–6, 2014.

[38] M. S. Demir, Ö. F. Gemici, and M. Uysal, "Genetic algortihm based resource allocation technique for vlc networks," in *Proc. IEEE Signal Processing and Communications Applications Conference (SIU)*, pp. 1–4, 2017.

[39] B. Ghimire and H. Haas, "Resource allocation in optical wireless networks," in *Proc. IEEE International Symposium on Personal Indoor and Mobile Radio Communications (PIMRC)*, pp. 1061–1065, 2011.

[40] X. Wu, M. Safari, and H. Haas, "Bidirectional allocation game in visible light communications," in *Proc. IEEE Vehicular Technology Conference (VTC)*, pp. 1–5, 2016.

[41] M. Kafafy, Y. Fahmy, M. Abdallah, and M. Khairy, "Power efficient downlink resource allocation for hybrid RF/VLC wireless networks," in *Proc. IEEE Wireless Communications and Networking Conference (WCNC)*, pp. 1–6, 2017.

[42] X. Li, R. Zhang, and L. Hanzo, "Cooperative load balancing in hybrid visible light communications and WiFi," *IEEE Transactions on Communications*, vol. 63, no. 4, pp. 1319–1329, 2015.

[43] W. Wu, F. Zhou, and Q. Yang, "Dynamic network resource optimization in hybrid VLC and radio frequency networks," in *Proc. IEEE International Conference on Selected Topics in Mobile and Wireless Networking (MoWNeT)*, pp. 1–7, 2017.

[44] Y. Wang, X. Wu, and H. Haas, "Load balancing game with shadowing effect for indoor hybrid LiFi/RF networks," *IEEE Transactions on Wireless Communications*, vol. 16, no. 4, pp. 2366–2378, 2017.

[45] A. M. Abdelhady, O. Amin, A. Chaaban, B. Shihada, and M.-S. Alouini, "Downlink resource allocation for dynamic TDMA-based VLC systems," *IEEE Transactions on Wireless Communications*, vol. 18, no. 1, pp. 108–120, 2018.

[46] Y. Qiu, S. Chen, H.-H. Chen, and W. Meng, "Visible light communications based on CDMA technology," *IEEE Wireless Communications*, vol. 25, no. 2, pp. 178–185, 2017.

[47] Z. Chen, D. A. Basnayaka, and H. Haas, "Space division multiple access for optical attocell network using angle diversity transmitters," *Journal of Lightwave Technology*, vol. 35, no. 11, pp. 2118–2131, 2017.

[48] X. Ling, J. Wang, Z. Ding, C. Zhao, and X. Gao, “Efficient OFDMA for LiFi downlink,” *Journal of Lightwave Technology*, vol. 36, no. 10, pp. 1928–1943, 2018.

[49] C. Chen, D. A. Basnayaka, and H. Haas, “Downlink performance of optical attocell networks,” *Journal of Lightwave Technology*, vol. 34, no. 1, pp. 137–156, 2015.

[50] M. W. Eltokhey, M.-A. Khalighi, and Z. Ghassemlooy, “Multiple access techniques for VLC in large space indoor scenarios: a comparative study,” in *Proc. IEEE International Conference on Telecommunications (ConTEL)*, pp. 1–6, 2019.

[51] M. Hammouda, A. M. Vegni, H. Haas, and J. Peissig, “Resource allocation and interference management in OFDMA-based VLC networks,” *Physical Communication*, vol. 31, pp. 169–180, 2018.

[52] X. Ling, J. Wang, Z. Ding, C. Zhao, and X. Gao, “Efficient OFDMA for LiFi downlink,” *Journal of Lightwave Technology*, vol. 36, no. 10, pp. 1928–1943, 2018.

[53] W. Wu, F. Zhou, and Q. Yang, “Adaptive network resource optimization for heterogeneous VLC/RF wireless networks,” *IEEE Transactions on Communications*, vol. 66, no. 11, pp. 5568–5581, 2018.

[54] M. Hammouda, S. Akın, A. M. Vegni, H. Haas, and J. Peissig, “Link selection in hybrid RF/VLC systems under statistical queueing constraints,” *IEEE Transactions on Wireless Communications*, vol. 17, no. 4, pp. 2738–2754, 2018.

[55] F. Jin, R. Zhang, and L. Hanzo, “Resource allocation under delay-guarantee constraints for heterogeneous visible-light and RF femtocell,” *IEEE Transactions on Wireless Communications*, vol. 14, no. 2, pp. 1020–1034, 2014.

[56] F. Wang, Z. Wang, C. Qian, L. Dai, and Z. Yang, "Efficient vertical handover scheme for heterogeneous VLC-RF systems," *Journal of Optical Communications and Networking*, vol. 7, no. 12, pp. 1172–1180, 2015.

[57] Y. Wang and H. Haas, "Dynamic load balancing with handover in hybrid Li-Fi and Wi-Fi networks," *Journal of Lightwave Technology*, vol. 33, no. 22, pp. 4671–4682, 2015.

[58] A. M. Vegni and T. D. C. Little, "Handover in VLC systems with cooperating mobile devices," in *Proc. IEEE International Conference on Computing, Networking and Communications (ICNC)*, pp. 126–130, 2012.

[59] T. Nguyen, Y. M. Jang, and M. Z. Chowdhury, "A pre-scanning-based link switching scheme in visible light communication networks," in *Proc. IEEE International Conference on Ubiquitous and Future Networks (ICUFN)*, pp. 366–369, 2013.

[60] M. Rahaim and T. D. C. Little, "SINR analysis and cell zooming with constant illumination for indoor VLC networks," in *Proc. IEEE International Workshop on Optical Wireless Communications (IWOW)*, pp. 20–24, 2013.

[61] T. C. Bui, S. Kiravittaya, N. H. Nguyen, N. T. Nguyen, and K. Spirinmanwat, "LEDs configuration method for supporting handover in visible light communication," in *Proc. IEEE Region 10 Conference (TENCON)*, pp. 1–6, 2014.

[62] S. Pergoloni, M. Biagi, S. Colonnese, R. Cusani, and G. Scarano, "Optimized LEDs footprinting for indoor visible light communication networks," *IEEE Photonics Technology Letters*, vol. 28, no. 4, pp. 532–535, 2016.

[63] E. Dinc, O. Ergul, and O. B. Akan, "Soft handover in OFDMA based visible light communication networks," in *Proc. IEEE Vehicular Technology Conference (VTC)*, pp. 1–5, 2015.

[64] K. Zheng, Q. Zheng, P. Chatzimisios, W. Xiang, and Y. Zhou, "Heterogeneous vehicular networking: a survey on architecture, challenges, and solutions," *IEEE communications surveys & tutorials*, vol. 17, no. 4, pp. 2377–2396, 2015.

[65] J. Guo, B. Song, Y. He, F. R. Yu, and M. Sookhak, "A survey on compressed sensing in vehicular infotainment systems," *IEEE Communications Surveys & Tutorials*, vol. 19, no. 4, pp. 2662–2680, 2017.

[66] S. Chen, J. Hu, Y. Shi, and L. Zhao, "LTE-V: a TD-LTE-based V2X solution for future vehicular network," *IEEE Internet of Things Journal*, vol. 3, no. 6, pp. 997–1005, 2016.

[67] K. Abboud, H. A. Omar, and W. Zhuang, "Interworking of DSRC and cellular network technologies for V2X communications: a survey," *IEEE Transactions on Vehicular Technology*, vol. 65, no. 12, pp. 9457–9470, 2016.

[68] M. Uysal, Z. Ghassemlooy, A. Bekkali, A. Kadri, and H. Menouar, "Visible light communication for vehicular networking: performance study of a V2V system using a measured headlamp beam pattern model," *IEEE Vehicular Technology Magazine*, vol. 10, no. 4, pp. 45–53, 2015.

[69] J.-H. Yoo, J.-S. Jang, J. Kwon, H.-C. Kim, D.-W. Song, and S.-Y. Jung, "Demonstration of vehicular visible light communication based on LED headlamp," *International Journal of Automotive Technology*, vol. 17, no. 2, pp. 347–352, 2016.

[70] A.-M. Căilean and M. Dimian, "Current challenges for visible light communications usage in vehicle applications: a survey," *IEEE Communications Surveys & Tutorials*, vol. 19, no. 4, pp. 2681–2703, 2017.

[71] A. Bazzi, B. M. Masini, A. Zanella, and A. Calisti, “Visible light communications as a complementary technology for the internet of vehicles,” *Computer Communications*, vol. 93, pp. 39–51, 2016.

[72] S. Liang, Y. Zhang, B. Fan, and H. Tian, “Multi-attribute vertical handover decision-making algorithm in a hybrid vlc-femto system,” *IEEE Communications Letters*, vol. 21, no. 7, pp. 1521–1524, 2017.

[73] M. D. Soltani, H. Kazemi, M. Safari, and H. Haas, “Handover modeling for indoor Li-Fi cellular networks: The effects of receiver mobility and rotation,” in *Proc. IEEE Wireless Communications and Networking Conference (WCNC)*, pp. 1–6, 2017.

[74] M. Hammouda, J. Peissig, and A. M. Vegni, “Design of a cognitive vlc network with illumination and handover requirements,” in *Proc. IEEE International Conference on Communications Workshops (ICC Workshops)*, pp. 451–456, 2017.

[75] X. Wu and H. Haas, “Handover skipping for LiFi,” *IEEE Access*, vol. 7, pp. 38369–38378, 2019.

[76] C. Yan, Y. Xu, J. Shen, and J. Chen, “A combination of vlc and wifi based indoor wireless access network and its handover strategy,” in *Proc. IEEE International Conference on Ubiquitous Wireless Broadband (ICUWB)*, pp. 1–4, 2016.

[77] M. S. Saud and M. Katz, “Implementation of a hybrid optical-RF wireless network with fast network handover,” in *Proc. European Wireless Conference*, pp. 1–6, 2017.

[78] P. Arunachalam and N. Kumar, “Visible light communication and radio network for vehicular environment,” in *Proc. IEEE International Conference on

Advances in Electronics, Computers and Communications (ICAECC), pp. 1–5, 2018.

[79] E. Torres-Zapata, V. Guerra, J. Rabadan, R. Perez-Jimenez, and J. M. Luna-Rivera, "Vehicular communications in tunnels using vlc," in *Proc. IEEE International Conference on Telecommunications (ConTEL)*, pp. 1–6, 2019.

[80] Q.-H. Dang and M. Yoo, "Handover procedure and algorithm in vehicle to infrastructure visible light communication," *IEEE Access*, vol. 5, pp. 26466–26475, 2017.

[81] N. Zhu, Z. Xu, Y. Wang, H. Zhuge, and J. Li, "Handover method in visible light communication between the moving vehicle and multiple LED streetlights," *Optik-International Journal for Light and Electron Optics*, vol. 125, no. 14, pp. 3540–3544, 2014.

[82] M. S. Demir and M. Uysal, "A cross-layer design for dynamic resource management of VLC networks," *IEEE Transactions on Communications*, vol. 69, no. 3, pp. 1858–1867, 2021.

[83] M. S. Demir, H. B. Eldeeb, and M. Uysal, "CoMP-based dynamic handover for vehicular VLC networks," *IEEE Communications Letters*, vol. 24, no. 9, pp. 2024–2028, 2020.

[84] M. S. Demir, S. M. Sait, and M. Uysal, "Unified resource allocation and mobility management technique using particle swarm optimization for VLC networks," *IEEE Photonics Journal*, vol. 10, no. 6, pp. 1–9, 2018.

[85] M. S. Demir, F. Miramirkhani, and M. Uysal, "Handover in VLC networks with coordinated multipoint transmission," in *Proc. IEEE International Black Sea Conference on Communications and Networking (BlackSeaCom)*, pp. 1–5, 2017.

[86] R. C. Kizilirmak, O. Narmanlioglu, and M. Uysal, "Centralized light access network (C-LiAN): a novel paradigm for next generation indoor VLC networks," *IEEE Access*, vol. 5, pp. 19703–19710, 2017.

[87] C. Bettstetter, G. Resta, and P. Santi, "The node distribution of the random waypoint mobility model for wireless ad hoc networks," *IEEE Transactions on Mobile Computing*, vol. 2, no. 3, pp. 257–269, 2003.

[88] R. Jain, D.-M. Chiu, and W. R. Hawe, *A quantitative measure of fairness and discrimination for resource allocation in shared computer system.* Eastern Research Laboratory, Digital Equipment Corporation Hudson, MA, 1984.

[89] C. Chen, M. Ijaz, D. Tsonev, and H. Haas, "Analysis of downlink transmission in DCO-OFDM-based optical attocell networks," in *Proc. IEEE Global Communications Conference (GLOBECOM)*, pp. 2072–2077, 2014.

[90] T. Matsui, K. Kato, M. Sakawa, T. Uno, and K. Matsumoto, "Particle swarm optimization for nonlinear integer programming problems," in *Proc. International MultiConference of Engineers and Computer Scientists*, pp. 1874–1877, 2008.

[91] J. Kennedy, "Particle swarm optimization," in *Encyclopedia of machine learning*, pp. 760–766, Springer, 2011.

[92] A. Salman, I. Ahmad, and S. Al-Madani, "Particle swarm optimization for task assignment problem," *Microprocessors and Microsystems*, vol. 26, no. 8, pp. 363–371, 2002.

[93] A. Basgumus, M. Namdar, G. Yilmaz, and A. Altuncu, "Performance comparison of the differential evolution and particle swarm optimization algorithms in free-space optical communications systems," *Advances in Electrical and Computer Engineering*, vol. 15, no. 2, pp. 17–22, 2015.

[94] S. M. Sait and H. Youssef, *Iterative Computer Algorithms with Applications in Engineering: Solving Combinatorial Optimization Problems*. IEEE Computer Society Press, 1999.

[95] S. Dimitrov, S. Sinanovic, and H. Haas, "Signal shaping and modulation for optical wireless communication," *Journal of Lightwave Technology*, vol. 30, no. 9, pp. 1319–1328, 2012.

[96] U. F. Siddiqi, S. M. Sait, M. S. Demir, and M. Uysal, "Resource allocation for visible light communication systems using simulated annealing based on a problem-specific neighbor function," *IEEE Access*, vol. 7, pp. 64077–64091, 2019.

[97] O. Amin, B. Gedik, and M. Uysal, "Channel estimation for amplify-and-forward relaying: cascaded against disintegrated estimators," *IET Communications*, vol. 4, no. 10, pp. 1207–1216, 2010.

[98] H. Kazemi and H. Haas, "Downlink cooperation with fractional frequency reuse in DCO-OFDMA optical attocell networks," in *Proc. IEEE International Conference on Communications (ICC)*, pp. 1–6, 2016.

[99] L. Yin and H. Haas, "Physical-layer security in multiuser visible light communication networks," *IEEE Journal on Selected Areas in Communications*, vol. 36, no. 1, pp. 162–174, 2017.

[100] M. J. Neely, "Stochastic network optimization with application to communication and queueing systems," *Synthesis Lectures on Communication Networks*, vol. 3, no. 1, pp. 1–211, 2010.

[101] Y. Guo, Q. Yang, J. Liu, and K. S. Kwak, "Cross-layer rate control and resource allocation in spectrum-sharing OFDMA small-cell networks with delay constraints," *IEEE Transactions on Vehicular Technology*, vol. 66, no. 5, pp. 4133–4147, 2016.

[102] L. Georgiadis, M. J. Neely, and L. Tassiulas, "Resource Allocation and Cross-Layer Control in Wireless Networks," *Foundations and Trends in Networking*, vol. 1, no. 1, pp. 1–144, 2005.

[103] L. A. Wolsey and G. L. Nemhauser, *Integer and combinatorial optimization*. John Wiley & Sons, 1999.

[104] J. Dréo, A. Pétrowski, P. Siarry, and E. Taillard, *Metaheuristics for hard optimization: methods and case studies*. Springer Science & Business Media, 2006.

[105] Ö. F. Gemici, F. Kara, İ. Hökelek, and H. A. Çırpan, "User scheduling and power allocation for nonfull buffer traffic in noma downlink systems," *International Journal of Communication Systems*, vol. 32, no. 1, p. e3834, 2019.

[106] J. Oh and C. Wu, "Genetic-algorithm-based real-time task scheduling with multiple goals," *Journal of Systems and Software*, vol. 71, no. 3, pp. 245–258, 2004.

[107] P. K. Muhuri, A. Rauniyar, and R. Nath, "On arrival scheduling of real-time precedence constrained tasks on multi-processor systems using genetic algorithm," *Future Generation Computer Systems*, vol. 93, pp. 702–726, 2019.

[108] M. F. Torquato and M. A. Fernandes, "High-performance parallel implementation of genetic algorithm on FPGA," *Circuits, Systems, and Signal Processing*, vol. 38, no. 9, pp. 4014–4039, 2019.

[109] E. Hahne, "Round-robin scheduling for max-min fairness in data networks," *IEEE Journal on Selected Areas in Communications*, vol. 9, no. 7, pp. 1024–1039, 1991.

[110] S. A. AlQahtani and M. Alhassany, "Comparing different LTE scheduling schemes," in *Proc. IEEE International Wireless Communications and Mobile Computing Conference (IWCMC)*, pp. 264–269, 2013.

[111] 3GPP, "Technical specification group radio access network; feasibility study for further advancements for E-UTRA (LTE-Advanced)," Tech. Rep. 36.912, 2011.

[112] C. Chen, D. Tsonev, and H. Haas, "Joint transmission in indoor visible light communication downlink cellular networks," in *Proc. IEEE Globecom Workshops (GC Wkshps)*, pp. 1127–1132, 2013.

[113] *Lighting of indoor work places.* International Standard. ISO 8995:2002 CIE S 008/E-2001.

[114] J. M. Kahn and J. R. Barry, "Wireless infrared communications," *Proceedings of the IEEE*, vol. 85, no. 2, pp. 265–298, 1997.

[115] Vestel Emphesis. http://www.vestelledlighting.com. [Accessed: May 11, 2021].

[116] M. Elamassie, M. Karbalayghareh, F. Miramirkhani, R. C. Kizilirmak, and M. Uysal, "Effect of fog and rain on the performance of vehicular visible light communications," in *Proc. IEEE Vehicular Technology Conference (VTC)*, pp. 1–6, 2018.

[117] 3GPP, "Evolved universal terrestrial radio access (E-UTRA); radio resource control (RRC); protocol specification," Tech. Rep. 36.331, 2017.

[118] K. D. C. Silva, Z. Becvar, and C. R. L. Frances, "Adaptive hysteresis margin based on fuzzy logic for handover in mobile networks with dense small cells," *IEEE Access*, vol. 6, pp. 17178–17189, 2018.

[119] A. Nakano and T. Saba, "A handover scheme based on signal power of coordinated base stations for CoMP joint processing systems," in *Proc. IEEE International Conference on Signal Processing and Communication Systems (ICSPCS)*, pp. 1–6, 2014.

VITA

M. Selim Demir received the B.Sc. degree in electronics and communication engineering from Istanbul Technical University, İstanbul, Turkey, in 2007 and the M.Sc. degree in electrical engineering from University of Columbia, New York, USA, in 2010. He is currently pursuing the Ph.D. degree under the supervision of Prof. Murat Uysal at Özyeğin University, İstanbul, Turkey. Since 2011, he has been a researcher at TÜBİTAK BİLGEM, where he participated in several network based projects. His current research interests include optical wireless communications, visible light communications, wireless mobile networks, relay networks, and deterministic networks.